LUND UNIVERSITY

A 9-DOF Tractor-Semitrailer Dynamic Handling Model for Advanced Chassis Control Studies

Gäfvert, Magnus; Lindgärde, Olof

2001

A 9-DOF Tractor-Semitrailer Dynamic Handling Model for Advanced Chassis Control Studies

Magnus Gäfvert
Olof Lindgärde[†]

[†]Volvo Technological Development
Sweden
Department of Automatic Control
Lund Institute of Technology, Sweden

December 2001

Department of Automatic Control Lund Institute of Technology Box 118 SE-221 00 Lund Sweden	*Document name* INTERNAL REPORT
	Date of issue December 2001
	Document Number ISRN LUTFD2/TFRT--7597--SE

Author(s)
Magnus Gäfvert
Olof Lindgärde

Supervisor

Sponsoring organization

Title and subtitle
A 9-DOF Tractor-Semitrailer Dynamic Handling Model for Advanced Chassis Control Studies.
(En dynamisk manövermodell med 9 frihetsgrader av en dragbil med semitrailer för studier av avancerad chassireglering).

Abstract
A nonlinear dynamic handling model for a tractor-semitrailer combination vehicle is presented in this report. The equations of motion are derived from the fundamental equations of dynamics in Euler's formulation without approximations. The model is modular in the sense that it is easy to change axle configuration, tyre model, suspension model, or to add new features. The primary aim of the model is simulations of handling scenarios with active yaw control, using unilateral braking and possibly tractor rear wheel steering. Other applications of the model may include real-time hardware-in-the-loop simulations of tractor-semitrailer handling scenarios. The model is formulated as a state-space model that may be implemented in standard simulation environments. A Simulink implementation is presented. Simulation results are compared with experiments to validate the model.

Keywords

Classification system and/or index terms (if any)

Supplementary bibliographical information

The report may be ordered from the Department of Automatic Control or borrowed through:
University Library 2, Box 3, SE-221 00 Lund, Sweden
Fax +46 46 222 44 22   E-mail ub2@ub2.se

Contents

1. Introduction

This report is part of the DICOSMOS2 project, under the Swedish NUTEK (VINNOVA) Complex Techical Systems Program. DICOSMOS2 is a joint effort between the Department of Automatic Control (LTH), Mechatronics/Department of Machine Design (KTH), the Department of Computer Engineering (Chalmers), and Volvo Technological Development (VTD). The project is aimed at the study of distributed control of safety-critical motion systems. Part of the DICOSMOS2 is a study on the design of distributed real-time control systems on vehicles, initiated by VTD. An active yaw-control system for a tractor-semitrailer commercial vehicle, see Figure 1, was selected as a case study. The present work is part of the results from the case study. More results are found in [SCG00, CGS00, GSC00, Gäf01]. In this report a nonlinear dynamic handling model for a tractor-semitrailer combination vehicle is derived. The equations of motion are derived from the fundamental equations of dynamics in Euler's formulation without approximations. The primary aim of the model is validation simulations of handling scenarios with active yaw control, using unilateral braking and possibly tractor rear wheel steering. The applications of the model are not limited to this domain, but may prove useful in other areas of tractor-semitrailer handling simulations. The model is formulated as a state-space model that may be implemented in standard simulation environments. A Simulink implementation is presented. Simulation results are compared with experiments to validate the model.

Figure 1   A Volvo FH12 tractor-semitrailer vehicle on the Öresund bridge. *(Courtesy of Volvo Truck Corporation.)*

1.1 Motivation

There are many existing models for simulation of tractor-semitrailer dynamics. They vary in a wide range of complexity from large multi-body system models with hundreds of degrees of freedom (DOFs), to small 3-DOF bicycle models. It is normally desirable to use the smallest possible models that fit a particular purpose, since they have less parameters, re-

quire less computational power, thus simulation time, and are easier to understand.

In yaw-control applications the lateral, longitudinal, and yaw motions of the vehicle are of primary interest. These motions are driven mainly by the tire-road contact forces. The contact forces depend on lateral and longitudinal motion of the vehicle, and on the vertical contact forces. The simplest possible model to use would then be a 4-DOF model: longitudinal, lateral, tractor yaw, and semitrailer yaw motion. It is unfortunately difficult to include a good description of tire-road vertical forces in such a model. These vertical forces vary with load transfer that results from inertial forces generated by the acceleration of vehicle masses. For commercial heavy vehicles this load transfer is large because of the high location of the center of mass (CM). Apart from using static load balance equations to compute the vertical forces, it is possible to use body accelerations to model load transfer. That approach was used in the previous work [GSC00].

These models do still not capture the real effects of load transfer. On real vehicles the suspension systems have great influence on the load transfer. They introduce a phase lag between the planar motion of the vehicle axles, or unsprung masses, and the vertical tire-road forces. To capture this phenomenon correctly it is necessary to use a model divided into sprung and unsprung masses, that are connected by the suspension system. When adding the sprung masses additional freedoms are introduced. Some models include only the additional roll freedom, which would be sufficient for modeling lateral motion at constant longitudinal velocity. In this work the choice became to include all heave, roll, and pitch motions of the sprung masses, thus introducing five additional DOFs (the heave freedom is common for the tractor and the semitrailer). The reason for this is that inclusion of pitch motion results in a more accurate description of longitudinal load transfer. The methods used for deriving the equations of motion do not become more difficult to use with these freedoms. The main effect is that already large expressions become larger. Since computer algebra tools was used this did not pose any real problems.

The reasons for deriving a new model instead of using an existing are several: Many previous models were derived in the 60s and 70s. These were derived by hand and therefore often subject to approximations that are not necessary with computer-algebra based methods available today. Furthermore, some equations were too large to solve analytically, and were thus left to numerical solution by iterative methods in the model implementations. This increases the computational complexity of the model, and may severely slow down simulations. These early models are also published as very large equations that are error-prone to implement in a simulation environment. Still these models provide good sources of knowledge when deriving a new model. Recent models are often of large complexity with many DOFs. Popular modeling environments are multi-body system software such as Adams. These often result in detailed models far beyond the needed level for handling simulations. They are useful to study structural forces and displacements on the vehicle body. The vast number of parameters in the multi-body models also makes them inappropriate to use when many different vehicle configurations are used. There are also recent intermediate DOF handling models, such as the commercial TruckSim software based on the AutoSim package. A drawback with those are that they are targeted at engineers rather than researchers. They are very easy to use

when working with conventional vehicles, but have less support for unconventional designs.

The present model is also targeted at future real-time simulation applications. A possible use would be in hardware-in-the-loop simulations for evaluating various control equipment. This means that algebraic relations requiring iterative solutions during simulation have been avoided.

1.2 Related Work

In the 60s and 70s there was an interest in handling-oriented models of tractor-semitrailer vehicles. The focus was then stability, and in particular jack-knifing behaviour of the vehicles. Early work was performed by Ellis [Ell69, Ell88, Ell94], who presents a 4-DOF nonlinear planar dynamic model of the tractor-semitrailer vehicle. An extension to the model includes roll freedom. A similar model is described in [Leu70]. Mikulcik [Mik68, Mik71] presents a more complete 8-DOF tractor-semitrailer model with longitudinal, lateral, heave and roll freedoms for the tractor-semitrailer, and separate yaw and pitch freedoms for the tractor and semitrailer respectively. A Fortran implementation of this model is also presented. The Fortran code includes several iterative algorithms for solving algebraic constraints. The model is used for analysis of jack-knifing behaviour. AutoSim [Say92] is a tool for generating efficient simulation code for a certain model class. The user only needs to describe the configuration of the system in terms of parameters. The equations of motion are solved for automatically. The major drawback with these tools in a research context is the closed environment they constitute. TruckSim generates models for conventional vehicles. Unconventional design that might be of interest for the research community are not included. The models may be extended with equations expressed in Lisp-like language, but in an environment where many experimental design are to be modeled it may be better with custom simulation models. Even though it may be a tedious work to dive into the actual equations of a model, that may provide a lot of insight into the model and its behaviour. A recent related work is [DYT00]. This work presents a 8-DOF (including wheel rotations) model of a car, intended for handling simulations similar to those targeted by the present work. The authors address the need for intermediate DOF models for handling studies. An AutoSim model is used for validation. In [CT95, CT00] a 5-DOF tractor-semitrailer model is derived using Lagrange methods. In this model a common roll freedom for the tractor and the semitrailer is introduced. The model is intended for the study of lateral dynamics control in the context of research on Automated Highway Systems. The model is evaluated with experimental data. In [RA95] a linear 3-DOF model of a tractor-semitrailer at constant speed is derived and implemented in Simulink. The objective is yaw-stability analysis simulations.

2. Model Overview

The configuration of the model is illustrated in Figure 2. The model consists of two sprung inertial bodies, connected by the hitch. The unsprung bodies (axles) are assumed to be massless. The hitch introduces algebraic constraints on the relative motion of the tractor and the semitrailer. These

algebraic relations are used to reduce the number of freedoms in the final equations of motion. Suspension characteristics at the wheel corners are included, as well as torsional stiffness of the tractor chassis frame. A realistic model of the kinematics and kinetics of the hitch is included. No approxi-
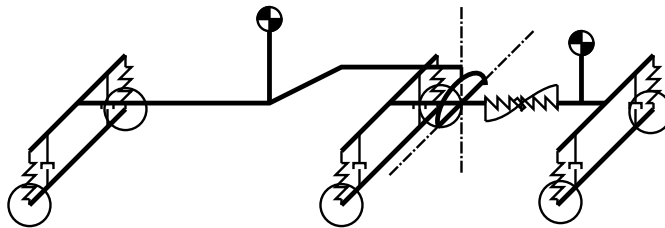
Figure 2 Vehicle configuration.

mations are made when deriving the equations of motion, other than the assumption on the vehicle configuration. Approximations are introduced in the modeling of the suspensions, axles, and tires.

The equations of motion are described in a reference system located in the hitch, that is aligned with the unsprung tractor frame, and fixed with respect to roll and pitch. This point on the vehicle has the unique property of being common for the tractor and semitrailer, which makes it possible to reduce the equations of motion using the kinematic constraints of the hitch. This particular choice of reference system results in reasonable small expressions that may be handled by computer-algebra tools such as Maple. The state variables that are used to describe the motion of the vehicle are listed in Table 1.

| State variable	Description
U	Longitudinal velocity of the hitch
V	Lateral velocity of the hitch
W	Vertical velocity of the hitch
r	Yaw-rate of the tractor
$\dot{\psi}$	Articulation angular velocity
$\dot{\phi}_s$	Tractor roll angular velocity
$\dot{\chi}_s$	Tractor pitch angular velocity
$\dot{\phi}_s$	Semitrailer roll angular velocity
$\dot{\chi}_s$	Semitrailer pitch angular velocity
Z	Pitch vertical position
ψ	Articulation angle
ϕ_t	Tractor roll angle
χ_t	Tractor pitch angle
ϕ_s	Semitrailer roll angle
χ_s	Semitrailer pitch angle

Table 1 State variables.

The model is modular in the sense that axle, suspension, and tire sub-

models are separate from the chassis dynamics. Hence it is easy to change axle and wheel configurations, to plug in different tire models, or to use different suspension models.

The analytical mechanics background of the modeling approach is described in detail in [LU84, FC93]. In the presentation below some notation has to be introduced. To help the reader a table of notations is included in Appendix A.

3. Vehicle configuration

The vehicle is divided into five separate parts as in Figure 3: The tractor sprung body $\mathcal{B}_{ts}$, the semitrailer sprung body $\mathcal{B}_{ss}$, the tractor unsprung body $\mathcal{B}_{tu}$, the semitrailer unsprung body $\mathcal{B}_{su}$, and the hitch body *, or rear tractor part, $\mathcal{B}_h$. The main reference system is the coordinate system S_{tu} that is attached to the tractor unsprung mass. It is aligned with the tractor, but does not roll nor pitch. The reference system S_{su} is similarly aligned with the semitrailer. The reference systems S_{ts}, S_{ss} and S_h are attached to the corresponding bodies. The reference system S_* is the earth-fixed inertial reference system. The origins of S_{tu}, S_{su}, S_{ts}, S_{ss} and S_h coincide and are located at the hitch, and is denoted O.
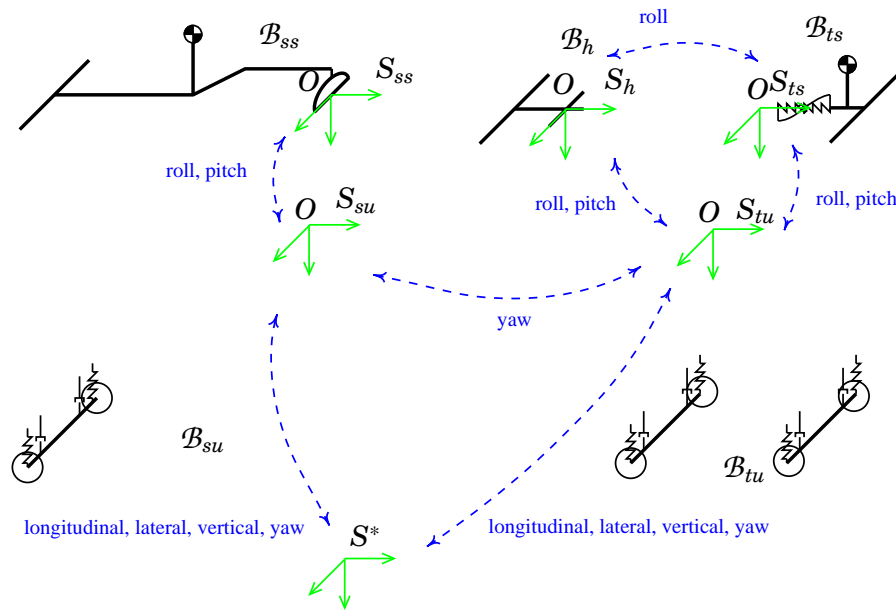
Figure 3 Vehicle parts with attached reference systems. The relative motion between reference systems are indicated with dashed lines with labels.

Vector variables are denoted with a bar. Vector representations with respect to a particular reference system is indicated by a superscript on the vector variable. Vectors are then represented as 3×1-matrices holding the components of the vector with respect to the reference system indicated by the superscript. The base vectors of the reference system S_i represented in

---

*Also denoted as "fifth wheel", or "king-pin".

S_i are denoted by $\vec{e}_x^i = (1,0,0)$, $\vec{e}_y^i = (0,1,0)$ and $\vec{e}_z^i = (0,0,1)$. Time derivatives of a vector with respect to a certain reference system is indicated with a subscript on the differential operator as $(d/dt)_i\, \bar{q}^j$. The shorthand notation of $\dot{\bar{q}}^j$ is used if $i = j$, i.e. the time derivative of $\bar{q}^j$ may be expressed as the time derivative of the components of $\bar{q}^j$.

The reference systems S_{tu} and S_{su} describe yaw rotation and translational longitudinal, lateral and vertical motion with respect to S_*. The angular velocities are $\bar{\omega}_{tu}^{tu} = (0,0,r)^T$ and $\bar{\omega}_{su}^{su} = (0,0,r')^T$ respectively. The velocity of O is $\bar{v}_O^{tu} = (U,V,W)$. The angle between S_{tu} and S_{su} is denoted the articulation angle, and is defined as $\psi = \int r\,dt - \int r'\,dt$. The reference system S_{ts} describes a pitch and roll motion with respect to S_{tu}, that is represented with the pitch angle χ_t and the roll angle ϕ_t. Correspondingly, S_{ss} describes a pitch and roll motion with respect to S_{su}, that is represented by χ_s and ϕ_s. The reference system S_h describes a pitch and roll motion with respect to S_{tu}, that is represented by χ_t and ϕ_h. In the modeling of non-articulated vehicles it is common to express the equations of motion in coordinate systems attached to the sprung body [KN00]. For articulated vehicles such as the tractor-semitrailer combination this may lead to difficulties in reducing the equations using the kinematic articulation constraints. For the tractor-semitrailer model the equations of motion are most conveniently expressed in the S_{tu} and S_{su} systems. Coordinate systems are oriented according to the SAE standard, with x pointing forward, y to the right, and z downwards, with respect to the vehicle forward direction.

4. Kinematics

In the derivation of the equations of motion for the vehicle it is necessary to have expressions for the acceleration of arbitrary points on the vehicle body.

4.1 Motion of a point in vehicle coordinates

Denote with S_* the earth fixed inertial reference frame, and with S_i the vehicle fixed non-inertial reference frame rotating with the angular velocity $\bar{\omega}_i$ and translating with the velocity $\bar{v}_O$, see Figure 4. For any vector $\bar{q}$ it
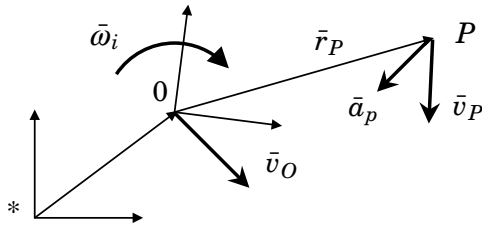
Figure 4 Acceleration of a particle in a rotating and translating reference frame.

holds that

$$\left(\frac{d}{dt}\right)_* \bar{q} = \left(\frac{d}{dt}\right)_i \bar{q} + \bar{\omega}_i \times \bar{q} \tag{1}$$

8

where '×' denote the cross-product operator. In particular the velocity of P with respect to S_* is expressed as the sum of the translational velocity of the vehicle reference system, and the time derivative of the position vector for P, $\bar{r}_P$:

$$\bar{v}_P = \bar{v}_O + \left(\frac{d}{dt}\right)_* \bar{r}_P = \bar{v}_O + \left(\frac{d}{dt}\right)_i \bar{r}_P + \bar{\omega}_i \times \bar{r}_P = \bar{v}_O + \dot{\bar{r}}_P + \bar{\omega}_i \times \bar{r}_P \quad (2)$$

The acceleration of P is computed by applying (1) on (2):

$$\bar{a}_P = \left(\frac{d}{dt}\right)_* \bar{v}_P = \left(\frac{d}{dt}\right)_i (\bar{v}_O + \dot{\bar{r}}_P + \bar{\omega}_i \times \bar{r}_P) + \bar{\omega}_i \times (\bar{v}_O + \dot{\bar{r}}_P + \bar{\omega}_i \times \bar{r}_P)$$
$$= \dot{\bar{v}}_O + \bar{\omega}_i \times \bar{v}_O + \dot{\bar{\omega}}_i \times \bar{r}_P + \bar{\omega}_i \times (\bar{\omega}_i \times \bar{r}_P) + 2\bar{\omega}_i \times \dot{\bar{r}}_P + \ddot{\bar{r}}_P \quad (3)$$

4.2 Coordinate transformations

Let $\bar{q}^{ts}$ be a vector representation in the tractor system S_{ts}. Then $\bar{q}^{tu} = \underline{R}_{ts}^{tu}\bar{q}^{ts}$ is the representation of this vector in S_{tu}. The rotational transformation $\underline{R}_{ts}^{tu}$ is defined as consecutive pitch and roll transformations with

$$\underline{R}_{ts}^{tu} = \begin{pmatrix} 1 & 0 & 0 \\ 0 & \cos\phi_t & -\sin\phi_t \\ 0 & \sin\phi_t & \cos\phi_t \end{pmatrix} \begin{pmatrix} \cos\chi_t & 0 & \sin\chi_t \\ 0 & 1 & 0 \\ -\sin\chi_t & 0 & \cos\chi_t \end{pmatrix} \quad (4)$$

Correspondingly a vector $\bar{q}^{ss}$ in the semitrailer system S_{ss} is represented in S_{su} as $\bar{q}^{su} = \underline{R}_{ss}^{su}\bar{q}^{ss}$ with

$$\underline{R}_{ss}^{su} = \begin{pmatrix} 1 & 0 & 0 \\ 0 & \cos\phi_s & -\sin\phi_s \\ 0 & \sin\phi_s & \cos\phi_s \end{pmatrix} \begin{pmatrix} \cos\chi_s & 0 & \sin\chi_s \\ 0 & 1 & 0 \\ -\sin\chi_s & 0 & \cos\chi_s \end{pmatrix} \quad (5)$$

Transformations between the semitrailer system S_{su} and the tractor system S_{tu} is described with $\bar{q}^{tu} = \underline{R}_{su}^{tu}\bar{q}^{su}$ with

$$\underline{R}_{su}^{tu} = \begin{pmatrix} \cos\psi & \sin\psi & 0 \\ -\sin\psi & \cos\psi & 0 \\ 0 & 0 & 1 \end{pmatrix} \quad (6)$$

The hitch kinematics is such that the roll angle ϕ_h of the tractor rear part $\mathcal{B}_h$ is given by

$$\phi_h = \phi_s \cos\psi + \chi_s \sin\psi \quad (7)$$

Thus it is equal to the roll angle of the semitrailer at zero articulation angle, and equal to the semitrailer pitch angle at 90 degrees articulation angle. The tractor rear part $\mathcal{B}_h$ always has the same pitch angle as the tractor front part $\mathcal{B}_{ts}$. Transformations between the tractor rear part system S_h and the tractor system S_{tu} is described with $\bar{q}^{tu} = \underline{R}_h^{tu}\bar{q}^h$ with

$$\underline{R}_h^{tu} = \begin{pmatrix} 1 & 0 & 0 \\ 0 & \cos\phi_h & -\sin\phi_h \\ 0 & \sin\phi_h & \cos\phi_h \end{pmatrix} \begin{pmatrix} \cos\chi_t & 0 & \sin\chi_t \\ 0 & 1 & 0 \\ -\sin\chi_t & 0 & \cos\chi_t \end{pmatrix} \quad (8)$$

4.3 Motion of a point on the tractor body

Let $\bar{r}_P^{ts}$ denote the position of an arbitrary point P on the tractor body $\mathcal{B}_{ts}$, expressed in the tractor fixed reference system S_{ts}. Then

$$\bar{r}_P^{tu} = \underline{R}_{ts}^{tu} \bar{r}_P^{ts} \tag{9}$$

The velocity of P is then

$$\bar{v}_P^{tu} = \bar{v}_O^{tu} + \left(\frac{d}{dt}\right)_{tu} \bar{r}_P^{tu} + \bar{\omega}_{tu}^{tu} \times \bar{r}_P^{tu} = \bar{v}_O^{tu} + \underline{\dot{R}}_{ts}^{tu} \bar{r}_P^{ts} + \bar{\omega}_{tu}^{tu} \times \underline{R}_{ts}^{tu} \bar{r}_P^{ts} \tag{10}$$

and the acceleration

$$\bar{a}_P^{tu} = \left(\frac{d}{dt}\right)_{tu} \bar{v}_P^{tu} + \bar{\omega}_{tu}^{tu} \times \bar{v}_P^{tu} = \dot{\bar{v}}_O^{tu} + \bar{\omega}_{tu}^{tu} \times \bar{v}_O^{tu} + \underline{\ddot{R}}_{ts}^{tu} \bar{r}_P^{ts} + \dot{\bar{\omega}}_{tu}^{tu} \times \underline{R}_{ts}^{tu} \bar{r}_P^{ts}$$
$$+ 2\bar{\omega}_{tu}^{tu} \times \underline{\dot{R}}_{ts}^{tu} \bar{r}_P^{ts} + \bar{\omega}_{tu}^{tu} \times \left(\bar{\omega}_{tu}^{tu} \times \underline{R}_{ts}^{tu} \bar{r}_P^{ts}\right) \tag{11}$$

4.4 Motion of a point on the semitrailer body

Let $\bar{r}_P^{ss}$ denote the position of an arbitrary point P on the semitrailer body $\mathcal{B}_{ss}$, expressed in the semitrailer fixed reference system S_{ss}. Then

$$\bar{r}_P^{su} = \underline{R}_{ss}^{su} \bar{r}_P^{ss} \tag{12}$$

The velocity of P is then

$$\bar{v}_P^{su} = \bar{v}_O^{su} + \left(\frac{d}{dt}\right)_{su} \bar{r}_P^{su} + \bar{\omega}_{su}^{su} \times \bar{r}_P^{su} = v_O^{su} + \underline{\dot{R}}_{ss}^{su} \bar{r}_P^{ss} + \bar{\omega}_{su}^{su} \times \underline{R}_{ss}^{su} \bar{r}_P^{ss} \tag{13}$$

and the acceleration

$$\bar{a}_P^{su} = \left(\frac{d}{dt}\right)_{su} \bar{v}_P^{su} + \bar{\omega}_{su}^{su} \times \bar{v}_P^{su} = \dot{\bar{v}}_O^{su} + \bar{\omega}_{su}^{su} \times \bar{v}_O^{su} + \underline{\ddot{R}}_{ss}^{su} \bar{r}_P^{ss} + \dot{\bar{\omega}}_{su}^{su} \times \underline{R}_{ss}^{su} \bar{r}_P^{ss}$$
$$+ 2\bar{\omega}_{su}^{su} \times \underline{\dot{R}}_{ss}^{su} \bar{r}_P^{ss} + \bar{\omega}_{su}^{su} \times \left(\bar{\omega}_{su}^{su} \times \underline{R}_{ss}^{su} \bar{r}_P^{ss}\right) \tag{14}$$

4.5 Motion of a point on the hitch body

Let $\bar{r}_P^{h}$ denote the position of an arbitrary point P on the hitch body $\mathcal{B}_{h}$, expressed in the rear tractor fixed reference system S_{h}. Then

$$\bar{r}_P^{tu} = \underline{R}_{h}^{tu} \bar{r}_P^{h} \tag{15}$$

The velocity of P is then

$$\bar{v}_P^{tu} = \bar{v}_O^{tu} + \left(\frac{d}{dt}\right)_{tu} \bar{r}_P^{tu} + \bar{\omega}_{tu}^{tu} \times \bar{r}_P^{tu} = \bar{v}_O^{tu} + \underline{\dot{R}}_{h}^{tu} \bar{r}_P^{h} + \bar{\omega}_{tu}^{tu} \times \underline{R}_{h}^{tu} \bar{r}_P^{h} \tag{16}$$

5. Kinetics

The free-body diagram of Figure 5 introduces the forces and moments that are used in the kinematic analysis. The bodies $\mathcal{B}_{ts}$ and $\mathcal{B}_{ss}$ carry the masses
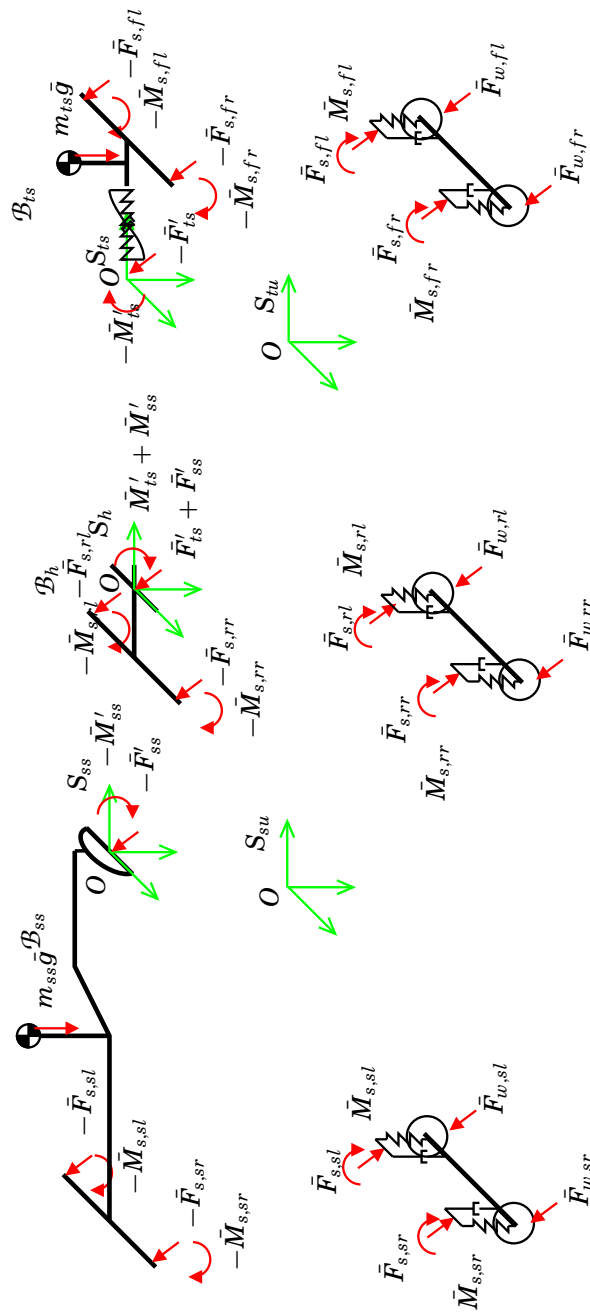
Figure 5 Vehicle free-body diagram.

m_{ts} and m_{ss}, with the inertial tensors $\underline{I}_{ts} = \int_{\mathcal{B}_{ts}} \left(r_P^2 \underline{1} - \bar{r}_P \bar{r}_P^T \right) dm_P$ and $\underline{I}_{ss} = \int_{\mathcal{B}_{ss}} \left(r_P^2 \underline{1} - \bar{r}_P \bar{r}_P^T \right) dm_P$ with respect to O.

The fundamental equations of dynamics in Euler's formulation postulates that

$$\bar{F} \equiv \int_{\mathcal{B}} d\bar{F}_P = \int_{\mathcal{B}} \bar{a}_P dm_P \tag{17a}$$

$$\bar{M}_O \equiv \int_{\mathcal{B}} \bar{r}_p \times d\bar{F}_P = \int_{\mathcal{B}} \bar{r}_P \times \bar{a}_P dm_P \tag{17b}$$

11

Thus for the tractor

$$\bar{F}_{ts} - \bar{F}'_{ts} = \int_{\mathcal{B}_{ts}} \bar{a}_P dm_P \qquad (18\text{a})$$

$$\bar{M}_{ts} - \bar{M}'_{ts} = \int_{\mathcal{B}_{ts}} \bar{r}_P \times \bar{a}_P dm_P \qquad (18\text{b})$$

where $\bar{F}_{ts}$ and $\bar{M}_{ts}$ are the sum of external moments and forces acting on $\mathcal{B}_{ts}$, and $\bar{F}'_{ts}$ and $\bar{M}'_{ts}$ are the internal reaction forces and moments from $\mathcal{B}_h$. Accordingly for the semitrailer

$$\bar{F}_{ss} - \bar{F}'_{ss} = \int_{\mathcal{B}_{ss}} \bar{a}_P dm_P \qquad (19\text{a})$$

$$\bar{M}_{ss} - \bar{M}'_{ss} = \int_{\mathcal{B}_{ss}} \bar{r}_P \times \bar{a}_P dm_P \qquad (19\text{b})$$

The static kinetic constraints that arise from the massless free body $\mathcal{B}_h$, are

$$\bar{F}'_{ts} + \bar{F}'_{ss} + \bar{F}_h = 0 \qquad (20\text{a})$$
$$\bar{M}'_{ts} + \bar{M}'_{ss} + \bar{M}_h = 0 \qquad (20\text{b})$$

where F_h and M_h are the external forces and moments acting on $\mathcal{B}_h$.

5.1 Elimination of internal forces and moments

The internal forces $\bar{F}'_{ts}$ and $\bar{F}'_{ss}$ may be eliminated by combining (18a), (19a) (20a), yielding

$$\bar{F}_{ts} + \bar{F}_{ss} + \bar{F}_h = \int_{\mathcal{B}_{ts}} \bar{a}_P dm_P + \int_{\mathcal{B}_{ss}} \bar{a}_P dm_P \qquad (21)$$

or

$$\bar{F}_{ts}^{tu} + \underline{R}_{su}^{tu} \bar{F}_{ss}^{su} + \bar{F}_h^{tu} = \int_{\mathcal{B}_{ts}} \bar{a}_P^{tu} dm_P + \underline{R}_{su}^{tu} \int_{\mathcal{B}_{ss}} \bar{a}_P^{su} dm_P \qquad (22)$$

when represented in S_{tu}. The integrals evaluate to terms including components of the center of gravity locations $\bar{r}_{CM,ts}^{ts}$ and $\bar{r}_{CM,ss}^{ss}$, and the masses m_{ts} and m_{ss}.

A little more care has to be taken when eliminating internal moments, because of the torque transfer characteristics of the hitch. Regard that the hitch transfer moment to the semitrailer along the $\bar{e}_x^{ss}$ axis at 0 articulation angle, and along the $\bar{e}_y^{ss}$ axis at 90 degrees articulation angle:

$$\bar{m}_{ss}^{ss} = m_{ss,xy}^{ss} \left(\cos\psi, \quad \sin\psi, \quad 0 \right)^T = m_{ss,xy}^{ss} \cos\psi\, \bar{e}_x^{ss} + m_{ss,xy}^{ss} \sin\psi\, \bar{e}_y^{ss} \qquad (23)$$

The moment transfer to the tractor is in all $\bar{e}_x^{ts}$, $\bar{e}_y^{ts}$ and $\bar{e}_z^{ts}$ directions, and is determined by the roll stiffness in the $\bar{e}_x^{ts}$ direction:

$$\bar{m}_{ts}^{ts} = \left(C_c \left(\phi_t - \phi_h \right), \quad m_{ts,y}^{ts}, \quad m_{ts,z}^{ts} \right)^T = C_c \left(\phi_t - \phi_h \right) \bar{e}_x^{ts} + m_{ts,y}^{ts} \bar{e}_y^{ts} + m_{ts,z}^{ts} \bar{e}_z^{ts} \qquad (24)$$

12

Now (20b) may be expressed in $\mathcal{B}_{tu}$ as

$$\underline{R}_{ts}^{tu}\left(C_c\left(\phi_t-\phi_h\right)\bar{e}_x^{ts}+m_{ts,y}^{ts}\bar{e}_y^{ts}+m_{ts,z}^{ts}\bar{e}_z^{ts}\right)$$
$$+\underline{R}_{ss}^{tu}\left(m_{ss,xy}^{ss}\cos\psi\,\bar{e}_x^{ss}+m_{ss,xy}^{ss}\sin\psi\,\bar{e}_y^{ss}\right)+\underline{R}_h^{tu}\bar{M}_h^h=0 \quad (25)$$

or

$$\left(\underline{R}_{ss}^{tu}\left(\cos\psi\,\bar{e}_x^{ss}+\sin\psi\,\bar{e}_y^{ss}\right)\quad \underline{R}_{ts}^{tu}\bar{e}_y^{ts}\quad \underline{R}_{ss}^{tu}\bar{e}_z^{ss}\right)\begin{pmatrix}m_{ss,xy}^{ss}\\m_{ts,y}^{ts}\\m_{ts,z}^{ts}\end{pmatrix}$$
$$=-\underline{R}_h^{tu}\bar{M}_h^h-C_c\left(\phi_t-\phi_h\right)\underline{R}_{ts}^{tu}\bar{e}_x^{ts} \quad (26)$$

which can be solved for $m_{ss,xy}^{ss}$, $m_{ts,y}^{ts}$ and $m_{ts,z}^{ts}$. Thus (18b) and (19b) may be represented as

$$\bar{M}_{ts}^{tu}-\underline{R}_{ts}^{tu}\bar{m}_{ts}^{ts}=\int_{\mathcal{B}_{ts}}\bar{r}_P^{tu}\times\bar{a}_P^{tu}dm_P \qquad (27)$$

$$\bar{M}_{ss}^{su}-\underline{R}_{ss}^{su}\bar{m}_{ss}^{ss}=\int_{\mathcal{B}_{ss}}\bar{r}_P^{su}\times\bar{a}_P^{su}dm_P \qquad (28)$$

The inertial tensors $\underline{I}_{ts}$ and $\underline{I}_{ss}$ expressed in the S_{ts} and S_{ss} systems gives the inertial matrices

$$\underline{I}_{ts}^{ts}=\int_{\mathcal{B}_{ts}}\left(r_P^{ts\,2}\underline{1}-\bar{r}_P^{ts}\bar{r}_P^{ts\,T}\right)dm_P$$
$$=\begin{pmatrix}\int_{\mathcal{B}_{ts}}(y_P^{ts})^2+(z_P^{ts})^2dm_P & -\int_{\mathcal{B}_{ts}}x_P^{ts}y_P^{ts}dm_P & -\int_{\mathcal{B}_{ts}}x_P^{ts}z_P^{ts}dm_P\\ -\int_{\mathcal{B}_{ts}}y_P^{ts}x_P^{ts}dm_P & \int_{\mathcal{B}_{ts}}(z_P^{ts})^2+(x_P^{ts})^2dm_P & -\int_{\mathcal{B}_{ts}}y_P^{ts}z_P^{ts}dm_P\\ -\int_{\mathcal{B}_{ts}}z_P^{ts}x_P^{ts}dm_P & -\int_{\mathcal{B}_{ts}}z_P^{ts}y_P^{ts}dm_P & \int_{\mathcal{B}_{ts}}(x_P^{ts})^2+(y_P^{ts})^2dm_P\end{pmatrix}$$

$$(29)$$

and

$$\underline{I}_{ss}^{ss}=\int_{\mathcal{B}_{ss}}\left(r_P^{ss\,2}\underline{1}-\bar{r}_P^{ss}\bar{r}_P^{ss\,T}\right)dm_P$$
$$=\begin{pmatrix}\int_{\mathcal{B}_{ss}}(y_P^{ss})^2+(z_P^{ss})^2dm_P & -\int_{\mathcal{B}_{ss}}x_P^{ss}y_P^{ss}dm_P & -\int_{\mathcal{B}_{ss}}x_P^{ss}z_P^{ss}dm_P\\ -\int_{\mathcal{B}_{ss}}y_P^{ss}x_P^{ss}dm_P & \int_{\mathcal{B}_{ss}}(z_P^{ss})^2+(x_P^{ss})^2dm_P & -\int_{\mathcal{B}_{ss}}y_P^{ss}z_P^{ss}dm_P\\ -\int_{\mathcal{B}_{ss}}z_P^{ss}x_P^{ss}dm_P & -\int_{\mathcal{B}_{ss}}z_P^{ss}y_P^{ss}dm_P & \int_{\mathcal{B}_{ss}}(x_P^{ss})^2+(y_P^{ss})^2dm_P\end{pmatrix}$$

$$(30)$$

The integrals in (27) and (28) evaluate to terms with elements from these inertial matrices.

Now (22), (27) and (28) forms the complete set of equations of motion for the tractor-semitrailer combination vehicle. A following section provides a more detailed description of the external forces that appear in these equations.

5.2 State equations

Equations (22), (27) and (28) may be written in matrix form as

$$
\begin{pmatrix}
\bar{F}_1^{tu} + \underline{R}_{su}^{tu} \bar{F}_{ss}^{su} + \bar{F}_h^{tu} \\
\bar{M}_{ts}^{tu} - \underline{R}_{ts}^{tu} \bar{M'}_{tu}^{tu} \\
\bar{M}_{ss}^{su} - \underline{R}_{ss}^{su} \bar{M'}_{ss}^{ss}
\end{pmatrix}
=
\begin{pmatrix}
\int_{\mathcal{B}_{ts}} \bar{a}_P^{tu} dm_P + \underline{R}_{su}^{tu} \int_{\mathcal{B}_{ss}} \bar{a}_P^{su} dm_P \\
\int_{\mathcal{B}_{ts}} \bar{r}_P^{tu} \times \bar{a}_P^{tu} dm_P \\
\int_{\mathcal{B}_{ss}} \bar{r}_P^{su} \times \bar{a}_P^{su} dm_P
\end{pmatrix}
\tag{31}
$$

Introduce the state vector

$$
\xi = (\xi_1, \xi_2) \tag{32a}
$$

with

$$
\xi_1 = (U, V, W, r, \dot{\psi}, \dot{\phi}_t, \dot{\chi}_t, \dot{\phi}_s, \dot{\chi}_s) \tag{32b}
$$

and

$$
\xi_2 = (Z, \psi, \phi_t, \chi_t, \phi_s, \chi_s) \tag{32c}
$$

The right hand side of (31) may be rewritten such that

$$
\begin{pmatrix}
\bar{F}_{ts}^{tu} + \underline{R}_{su}^{tu} \bar{F}_{ss}^{su} + \bar{F}_h^{tu} \\
\bar{M}_{ts}^{tu} - \underline{R}_{ts}^{tu} \bar{m}_{ts}^{ts} \\
\bar{M}_{ss}^{su} - \underline{R}_{ss}^{su} \bar{m}_{ss}^{ss}
\end{pmatrix}
= H(\xi) \frac{d\xi_1}{dt} - F(\xi)
\tag{33}
$$

The complete state equations are

$$
\frac{d\xi_1}{dt} = H(\xi)^{-1} \left(F(\xi) +
\begin{pmatrix}
\bar{F}_{ts}^{tu} + \underline{R}_{su}^{tu} \bar{F}_{ss}^{su} + \bar{F}_h^{tu} \\
\bar{M}_{ts}^{tu} - \underline{R}_{ts}^{tu} \bar{m}_{ts}^{ts} \\
\bar{M}_{ss}^{su} - \underline{R}_{ss}^{su} \bar{m}_{ss}^{ss}
\end{pmatrix}
\right)
\tag{34}
$$

$$
\frac{d\xi_2}{dt} = E\xi_1 \tag{35}
$$

with

$$
E =
\begin{pmatrix}
0 & 0 & 1 & 0 & 0 & 0 & 0 & 0 & 0 \\
0 & 0 & 0 & 1 & 0 & 0 & 0 & 0 & 0 \\
0 & 0 & 0 & 0 & 0 & 1 & 0 & 0 & 0 \\
0 & 0 & 0 & 0 & 0 & 0 & 1 & 0 & 0 \\
0 & 0 & 0 & 0 & 0 & 0 & 0 & 1 & 0 \\
0 & 0 & 0 & 0 & 0 & 0 & 0 & 0 & 1
\end{pmatrix}
\tag{36}
$$

The elements of the matrix $H(\xi)$ and the vector $F(\xi)$ are large expressions that need to be computed with computer algebra software such as Maple. The matrix $H(\xi)$ is not possible to invert analytically, since it would lead to *very* large expressions. Instead this matrix is computed numerically at each integration step, and inverted numerically.

The large expressions in the elements of $H(\xi)$ and $F(\xi)$ result from the cross-products of the position and acceleration vectors of Sections 4.3–4.4. The acceleration vectors also include first and second time derivatives of

the transformation matrices in Section 4.2. As an illustration of the size of the analytical expressions in the matrices, the number of terms in each element is given below.

$$
H: \begin{pmatrix}
3 & 1 & 1 & 5 & 2 & 1 & 2 & 2 & 2 \\
1 & 3 & 1 & 4 & 2 & 3 & 2 & 2 & 2 \\
1 & 1 & 2 & 1 & 1 & 3 & 2 & 3 & 2 \\
1 & 4 & 3 & 8 & 1 & 11 & 6 & 1 & 1 \\
4 & 1 & 2 & 11 & 1 & 6 & 8 & 1 & 1 \\
3 & 2 & 1 & 9 & 1 & 6 & 6 & 1 & 1 \\
4 & 4 & 3 & 8 & 8 & 1 & 1 & 11 & 6 \\
4 & 4 & 2 & 11 & 11 & 1 & 1 & 6 & 8 \\
5 & 5 & 1 & 9 & 9 & 1 & 1 & 6 & 6
\end{pmatrix}
\qquad
F: \begin{pmatrix}
12 \\ 15 \\ 14 \\ 41 \\ 42 \\ 34 \\ 74 \\ 79 \\ 57
\end{pmatrix}
\qquad (37)
$$

The terms are nonlinear expressions of the state variables.

5.3 External forces

The external forces that act on the vehicle are gravitational forces, tyre-road contact forces, and wind-drag forces. Wind-drag forces are proportional to the squared resultant wind velocity [KN00].

$$
\begin{pmatrix}
F_{wind,x} \\
F_{wind,y} \\
F_{wind,z}
\end{pmatrix}
=
\begin{pmatrix}
C_{aer,x} A_x \frac{\rho}{2} U_{wind,x}^2 \\
C_{aer,y} A_y \frac{\rho}{2} U_{wind,y}^2 \\
0
\end{pmatrix}
\qquad (38)
$$

where $C_{aer,x/y}$ are aerodynamic drag coefficients, $A_{x/y}$ front and side effective areas, and $U_{wind,x/y}$ the resultant wind velocity. The gravitational forces are

$$
\bar{F}_{g,ts} = \int_{\mathcal{B}_{ts}} \bar{g}\, dm_P = m_{ts} g \bar{e}_z^{tu} \qquad (39)
$$

$$
\bar{F}_{g,ss} = \int_{\mathcal{B}_{ss}} \bar{g}\, dm_P = m_{ss} g \bar{e}_z^{su} \qquad (40)
$$

The tyre-road contact forces are obtained from the tire model, which is described in a following section. These forces are transfered to the sprung chassis through the suspension, and depend on suspension characteristics and axle configurations. The suspension system determines the vertical forces as well as pitch and roll moments.

The axle and suspension kinetics are derived from analyzing the free-body diagram of Figure 6. The indices "f", "r" and "s" on the variables in the diagram denote front axle, rear axle and semitrailer axle. (There may be several of each sort.) The indices "l" and "r" denote the left or right side of axle[†]. The description of the axle kinetics is presented for an arbitrary axle. The axles kinetics is described in the S_{tu} and S_{su} for the tractor and semitrailer axles respectively. Axle indices are therefore dropped in the following.

[†]Even if the same index is used for "rear axle" and "right side", the meaning is always clear from the context.
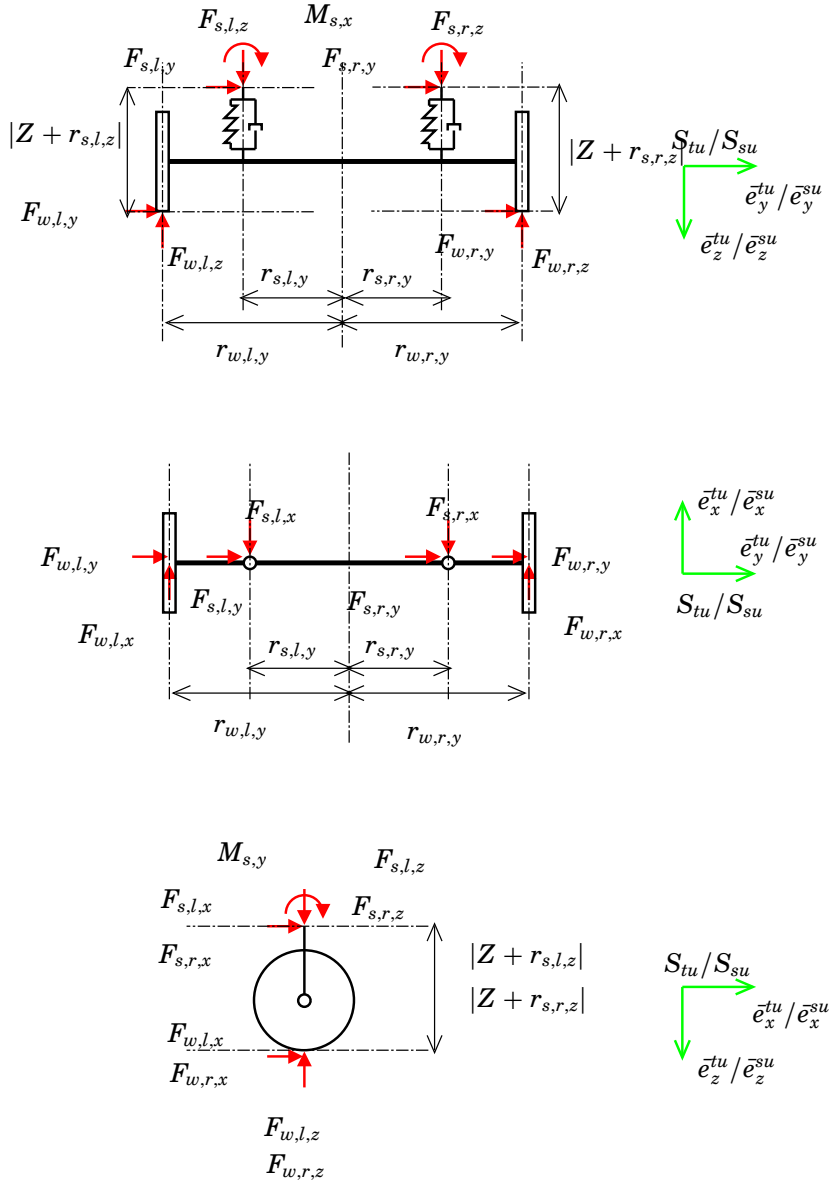
Figure 6 Tractor front axle and suspension kinetics. Tractor rear axle and semi-trailer axle have corresponding configurations.

Denote the suspension forces at corner $i \in \{l, r\}$ by $\bar{F}_{s,i}$, the suspension moments by $\bar{M}_{s,i}$, and the wheel forces by $\bar{F}_{w,i}$. Now $F_{s,i,z}$, $F_{w,i,x}$, $F_{w,i,y}$, $M_{s,i,x}$, $M_{s,i,z}$ may be expressed directly in terms of position and velocity of the suspension corner, which can be computed from the state variables, while $F_{s,i,x}$, $F_{s,i,y}$, $F_{w,i,z}$, $M_{s,i,y}$ need to be solved for. Since the axle and the body are two rigid bodies that have two supporting connections aligned in the $\bar{e}_y^{tu}$, $\bar{e}_y^{su}$ directions, there are no internal moments acting in the $\bar{e}_x^{tu}$, $\bar{e}_x^{su}$ and $\bar{e}_z^{tu}$, $\bar{e}_z^{su}$ directions. With an additional roll-stiffener an extra moment in the $\bar{e}_x^{tu}$, $\bar{e}_x^{su}$ direction may be added. Let $\bar{M}_{s,x} = \bar{M}_{s,l,x} + \bar{M}_{s,r,x}$ and $\bar{M}_{s,y} = \bar{M}_{s,l,y} + \bar{M}_{s,r,y}$ denote the lumped suspension moments on one axle. This reduces the number of free variables.

16

5.4 Axle balance equations

The tyre forces $F_{w,l,x}$, $F_{w,l,y}$, $F_{w,r,x}$, $F_{w,r,y}$ are assumed to be expressed as $F_{w,l,x} = F_{w,l,z}\mu_{l,x}$, $F_{w,l,y} = F_{w,l,z}\mu_{l,y}$, $F_{w,r,x} = F_{w,r,z}\mu_{r,x}$, $F_{w,r,y} = F_{w,r,z}\mu_{r,y}$, where $\mu_{l,x}$, $\mu_{l,y}$, $\mu_{r,x}$, $\mu_{r,y}$ are coefficients of friction given from the tyre model. This assumption is commented further at the end of this section.

Let $\Delta r_{s,l,z}$, $\Delta r_{s,r,z}$, $v_{s,l,z}$ and $v_{s,r,z}$ denote the suspension travel and velocity at the left and right suspension corners at a given time. These variables may be computed from the state variables using the transformations of Section 4. The vertical suspension forces may now be computed using any desired mapping. In this presentation we introduce the simple linear suspension

$$F_{s,l,z} = -C_s \Delta r_{s,l,z} - D_s v_{s,l,z} \tag{41a}$$

$$F_{s,r,z} = -C_s \Delta r_{s,r,z} - D_s v_{s,r,z} \tag{41b}$$

In the implementation of the model presented in this report nonlinear asymmetrical dampers based on lookup-tables are used.

The known suspension moments are

$$M_{s,x} = -C_r(\Delta r_{s,r,z} - \Delta r_{s,l,z}) \tag{42a}$$

$$M_{s,z} = 0 \tag{42b}$$

where an anti-roll bar with stiffness C_r is introduced to provide additional roll stiffness.

Balance of forces and moments result in the following set of equations:

$$
\begin{aligned}
F_{s,l,x} + F_{s,r,x} + F_{w,l,x} + F_{w,r,x} &= 0 & \text{(43a)} \\
F_{s,l,y} + F_{s,r,y} + F_{w,l,y} + F_{w,r,y} &= 0 & \text{(43b)} \\
F_{s,l,z} + F_{s,r,z} + F_{w,l,z} + F_{w,r,z} &= 0 & \text{(43c)} \\
-r_{s,l,z}F_{s,l,y} - r_{s,r,z}F_{s,r,y} + r_{s,l,y}F_{s,l,z} + r_{s,r,y}F_{s,r,z} + & & \\
r_{w,l,y}F_{w,l,z} + r_{w,r,y}F_{w,r,z} + M_{s,x} &= 0 & \text{(43d)} \\
r_{s,l,z}F_{s,l,x} + r_{s,r,z}F_{s,r,x} + M_{s,y} &= 0 & \text{(43e)} \\
-r_{s,l,y}F_{s,l,x} - r_{s,r,y}F_{s,r,x} - r_{w,l,y}F_{w,l,x} - r_{w,r,y}F_{w,r,x} &= 0 & \text{(43f)}
\end{aligned}
$$

Recall that the wheel forces $F_{w,l,y}$ and $F_{w,l,x}$ are assumed to depend linearly on the normal forces. Hence, the equations (43a–43f) can be rewritten as

$$F_{s,l,x} + F_{s,r,x} - \mu_{l,x}F_{w,l,z} - \mu_{r,x}F_{w,r,z} = 0 \tag{44a}$$

$$F_{s,l,y} + F_{s,r,y} - \mu_{l,y}F_{w,l,z} - \mu_{r,y}F_{w,r,z} = 0 \tag{44b}$$

$$F_{w,l,z} + F_{w,r,z} = -F_{s,l,z} - F_{s,r,z} \tag{44c}$$

$$
\begin{aligned}
-r_{s,l,z}F_{s,l,y} - r_{s,r,z}F_{s,r,y} + r_{w,l,y}F_{w,l,z} + r_{w,r,y}F_{w,r,z} = & & \text{(44d)} \\
-M_{s,x} - r_{s,l,y}F_{s,l,z} - r_{s,r,y}F_{s,r,z} &
\end{aligned}
$$

$$r_{s,l,z}F_{s,l,x} + r_{s,r,z}F_{s,r,x} + M_{s,y} = 0 \tag{44e}$$

$$r_{s,l,y}F_{s,l,x} + r_{s,r,y}F_{s,r,x} - r_{w,l,y}\mu_{l,x}F_{w,l,z} - r_{w,r,y}\mu_{r,x}F_{w,r,z} = 0 \tag{44f}$$

In addition, it is assumed that side forces are equally carried by the suspension

$$F_{s,l,y} = F_{s,r,y} \tag{45}$$

Equations (44a–44f) together with (45) give

$$
\begin{pmatrix}
1 & 1 & 0 & 0 & \mu_{l,x} & \mu_{r,x} & 0 \\
0 & 0 & 1 & 1 & \mu_{l,y} & \mu_{r,y} & 0 \\
0 & 0 & 0 & 0 & 1 & 1 & 0 \\
0 & 0 & -r_{s,l,z} & -r_{s,r,z} & r_{w,l,y} & r_{w,r,y} & 0 \\
r_{s,l,z} & r_{s,r,z} & 0 & 0 & 0 & 0 & 1 \\
r_{s,l,y} & r_{s,r,y} & 0 & 0 & r_{w,l,y}\mu_{l,x} & r_{w,r,y}\mu_{r,x} & 0 \\
0 & 0 & 1 & -1 & 0 & 0 & 0
\end{pmatrix}
$$

$$
\cdot
\begin{pmatrix}
F_{s,l,x} \\
F_{s,r,x} \\
F_{s,l,y} \\
F_{s,r,y} \\
F_{w,l,z} \\
F_{w,r,z} \\
M_{s,y}
\end{pmatrix}
=
\begin{pmatrix}
0 \\
0 \\
-F_{s,l,z} - F_{s,r,z} \\
-M_{s,x} - r_{s,l,y}F_{s,l,z} - r_{s,r,y}F_{s,r,z} \\
0 \\
0 \\
0
\end{pmatrix}
\qquad (46)
$$

Roll-over Conditions   During heavy cornering the right or left wheel may not stay in contact with the ground. The wheel normal force is then zero, i.e. $F_{w,l,z} = 0$ or $F_{w,r,z} = 0$, and the solution of the force and moment balance in Equation (46) is not valid. To still achieve at least approximately correct behaviour from the model under such conditions a simplistic solution is presented in this section. The basic idea is to replace the free variable ($F_{w,l,z}$ or $F_{w,r,z}$) that disappears from the balance equation with another. For this purpose the axle roll angle φ is introduced as a new degree of freedom. Two simplifying assumptions are also introduced to avoid a nonlinear axle balance equations that might require iterative solution methods: *(i)* It is assumed that spring characteristics are linear. *(ii)* The damper force does not depend on the roll velocity of the suspension axle $\dot{\varphi}$.

The case with $F_{w,l,z} = 0$, leading to $\varphi > 0$, is described in the following. (The case with $F_{w,r,z} = 0$ and $\varphi < 0$ is treated analogously.) The vertical suspension forces in (41a) and (41b) then become

$$
\begin{aligned}
F_{s,l,z} &= -C_s \left(\Delta r_{s,l,z} - (r_{w,r,y} - r_{s,l,y}) \sin(\varphi) \right) - D_s v_{s,l,z} \\
&= -C_s \Delta r_{s,l,z} - D_s v_{s,l,z} + C_s (r_{w,r,y} - r_{s,l,y}) \sin(\varphi) \\
&\equiv \bar{F}_{s,l,z} + k_l \sin(\varphi) \qquad\qquad\qquad\qquad\qquad (47a)
\end{aligned}
$$

$$
\begin{aligned}
F_{s,r,z} &= -C_s \left(\Delta r_{s,r,z} - (r_{w,r,y} - r_{s,r,y}) \sin(\varphi) \right) - D_s v_{s,r,z} \\
&= -C_s \Delta r_{s,r,z} - D_s v_{s,r,z} + C_s (r_{w,r,y} - r_{s,r,y}) \sin(\varphi) \\
&\equiv \bar{F}_{s,r,z} + k_r \sin(\varphi) \qquad\qquad\qquad\qquad\qquad (47b)
\end{aligned}
$$

By applying (47a) and (47b) to (44a)–(44f) the following set of linear equations is obtained:

18

$$
\begin{pmatrix}
1 & 1 & 0 & 0 & 0 & -\mu_{r,x} & 0 \\
0 & 0 & 1 & 1 & 0 & -\mu_{r,y} & 0 \\
0 & 0 & 0 & 0 & k_l + k_r & 1 & 0 \\
0 & 0 & -r_{s,l,z} & -r_{s,r,z} & r_{s,l,y}k_l + r_{s,r,y}k_r & r_{w,r,y} & 0 \\
r_{s,l,z} & r_{s,r,z} & 0 & 0 & 0 & 0 & 1 \\
r_{s,l,y} & r_{s,r,y} & 0 & 0 & 0 & -r_{w,r,y}\mu_{r,x} & 0 \\
0 & 0 & 1 & -1 & 0 & 0 & 0
\end{pmatrix}
$$

$$
\cdot
\begin{pmatrix}
F_{s,l,x} \\
F_{s,r,x} \\
F_{s,l,y} \\
F_{s,r,y} \\
\sin(\varphi) \\
F_{w,r,z} \\
M_{s,y}
\end{pmatrix}
=
\begin{pmatrix}
0 \\
0 \\
-\bar{F}_{s,l,z} - \bar{F}_{s,r,z} \\
-M_{s,x} - r_{s,l,y}\bar{F}_{s,l,z} - r_{s,r,y}\bar{F}_{s,r,z} \\
0 \\
0 \\
0
\end{pmatrix}
\qquad (48)
$$

Tires with Nonlinear Normal Force Dependence   If the assumptions on linear normal force dependence of the tire forces $F_{w,x} = F_{w,z}\mu_x$ and $F_{w,y} = F_{w,z}\mu_y$ do not hold, but instead the tire forces are described by general nonlinear functions $(F_{w,z}, \xi) \mapsto F_{w,x}$ and $(F_{w,z}, \xi) \mapsto F_{w,y}$, then this would lead to nonlinear algebraic relations. To compute the tire lateral forces one would need the tire vertical forces, and to compute the tire vertical forces, the lateral forces would be needed. This would need to be handled with iterative solution methods, and would increase the computational complexity. A way to handle this is to introduce a piecewise linear approximation as

$$
F_{w,x} = m_i + k_i F_{w,z}\mu_x, \qquad \text{with } i \text{ such that } F_{w,z} \in \mathcal{F}_i \qquad (49)
$$

A set of triples $\{(\mathcal{F}_i, m_i, k_i)\}$, $i \in 1, \ldots n$ where $\mathcal{F}_i$ is the interval of the normal force where the linear approximation is valid, is defined. Then the axle balance equations are solved for each i, and the solution for which the solved normal forces $F_{w,l,z}$, $F_{w,r,z}$ belongs the assumed interval $\mathcal{F}_i$ is chosen. This means solving a finite number (n) of axle balance equations and choosing one solution. The advantage is that this computation has a known computation time, which is not necessarily true for iterative methods. Often it is possible to find reasonably accurate piece-wise linear models of the normal load dependence.

6. Tire Models

The longitudinal tire slip λ is defined as

$$
\lambda = \frac{\omega R_w - u}{u} \qquad (50)
$$

where u, v are the longitudinal and lateral velocities of the wheel center expressed in a reference system aligned with the wheel, ω is the wheel

angular velocity, and R_w is the effective wheel radius. The lateral side-slip α is defined as

$$\tan \alpha = -\frac{v}{u} \tag{51}$$

Many tire models are formulated as mappings from λ, α and the tire vertical load $F_{w,z}$ to the longitudinal and lateral adhesion forces $F_{w,x}$ and $F_{w,y}$. The adhesion coefficients μ_x and μ_y are defined as

$$\mu_x = \frac{F_{w,x}}{F_{w,z}} \tag{52a}$$

$$\mu_y = \frac{F_{w,y}}{F_{w,z}} \tag{52b}$$

The adhesion force characteristics for a real tire at pure cornering and pure braking are shown in Figure 7. At combined braking and cornering
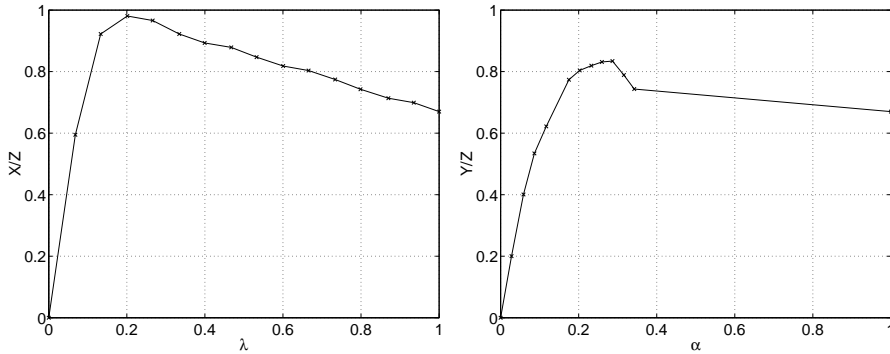
Figure 7 Experimental tire adhesion coefficients at pure braking and pure cornering. The last data value for the lateral adhesion coefficient is estimated as being equal to the longitudinal adhesion coefficient for $\lambda = 1$. The experimental data is obtained from Volvo Truck Corporation [Edl91][†].

the adhesion coefficients are reduced compared to pure braking and pure cornering. This is illustrated for a real tire in Figure 8. The choice of tire model depends on in which region the model is supposed to operate. For maneuvers with pure braking or pure cornering and small slips the tires behave approximately linearly and a simple tire model may suffice. At large slips or combined braking and cornering it may be necessary to use more sophisticated models. Two different models are presented in the following sections.

6.1 Linear Tire Model

The simplest tire model is the linear model

$$F_{w,x} = C_\lambda \lambda \tag{53a}$$

$$F_{w,y} = C_\alpha \alpha \tag{53b}$$

The model (53) has the drawbacks of not including limitations of available tire adhesion forces, and not modeling the coupling between longitudinal and lateral adhesion forces at combine cornering and braking. It may still be useful for modeling tire behaviour in the small-slip region.

20
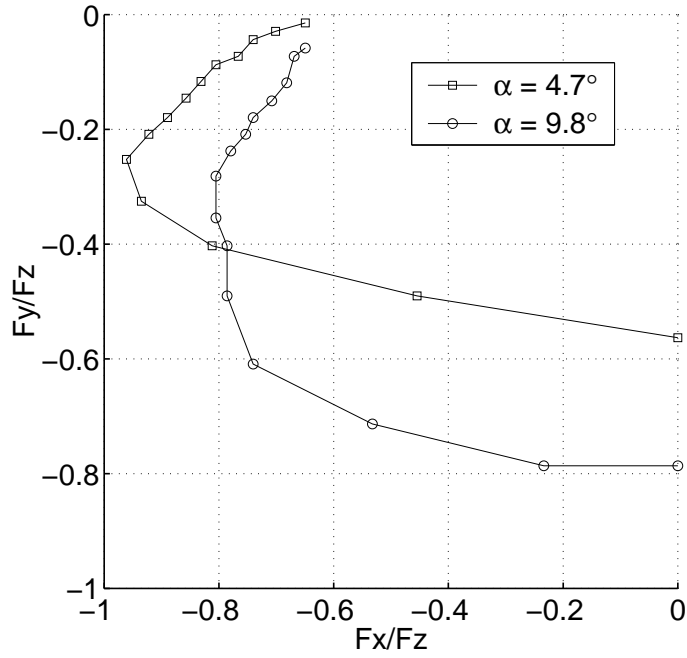
Figure 8 Experimental tire adhesion coefficients at combined braking and cornering for two fixed α and varying λ. The experimental data is obtained from Volvo Truck Corporation [Edl91][†].

6.2 Slip Circle Model

The *slip circle* model [SPP96] is a generic tyre model for combined braking and cornering based on models of pure braking and cornering. Introduce the dimensionless slip variable s

$$s = \sqrt{\lambda^2 + \sin^2 \alpha} \tag{54}$$

(It is common to describe the side-slip with the dimensionless entity $\sin \alpha$ instead of α. For small α the difference is negligible.) Define the slip angle β as

$$\tan \beta = \frac{\sin \alpha}{\lambda} \tag{55}$$

The tyre force is assumed to be counter-directed to the slip vector described by s and β.

Now introduce the pure cornering and braking mappings from slips to tyre forces $f : (\lambda, F_{w,z}) \mapsto F_{w,x}$ and $g : (\alpha, F_{w,z}) \mapsto F_{w,y}$. In the slip-circle model the magnitude of the combined tyre force is now described as

$$F = f(s) \cos^2 \beta + g(s) \sin^2 \beta \tag{56}$$

Now

$$F_{w,x} = F \cos \beta \tag{57a}$$

$$F_{w,y} = F \sin \beta \tag{57b}$$

21

It is seen that pure cornering and braking are restored for $\beta = 0$ and $\beta = \pi/2$. For other β the combined tyre forces lies on a curve that is "close" to an ellipse. The slip circle model is compared with experiments in Figure 9. The mappings f and g may be chosen as experimentally acquired
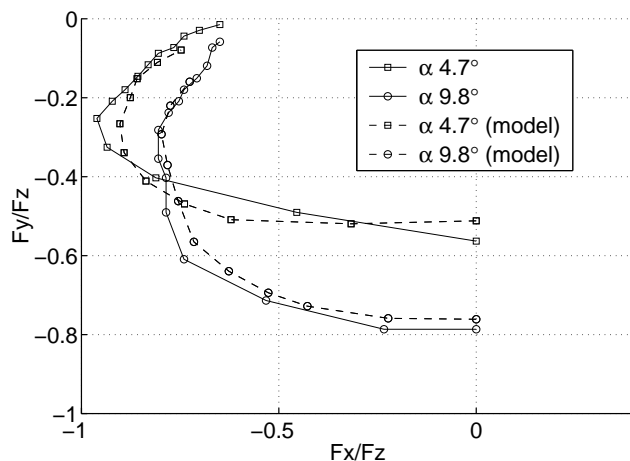
Figure 9 Slip circle model and experimental adhesion coefficients at combined braking and cornering for two fixed α and varying λ. The experimental data is obtained from Volvo Truck Corporation [Edl91][†].

lookup-tables.

7. Wheel Dynamics

The rotational dynamics of the wheels are modeled as

$$J_w \frac{d}{dt}\omega = M_\omega - R_w F_{w,x} \tag{58}$$

where J_w is the moment of inertia of the wheel, and M_ω the driving or braking moment.

In many cases the wheel rotational dynamics are not interesting to model, and the longitudinal slips λ may be used directly as inputs to the vehicle model.

8. Implementation

The general procedure to realize the dynamics described in Section 5 is to analytically compute the matrices $F(\xi)$ and $H(\xi)$ using computer algebra software. An automated tool to translate these expressions to a computer language supported by the simulation software is then used. In this work Maple was used to compute $F(\xi)$ and $H(\xi)$. Maple has support for translation of expressions to the programming language C. The expressions for $F(\xi)$ resulted in around 300 lines of C-code, and the expressions for $H(\xi)$ in around 200 lines. The generated C-files were included in Matlab mex-file

---

[†]The details on the tire experiments are classified corporate information.

functions defined to return the matrices as functions of the state ξ. The position, velocity and acceleration relations of Sections 4.3–4.5 was similarly computed in Maple and translated to mex-file functions. These relations are needed to compute suspension and wheel motion that are used for the axle balance equations of Section 5.4, and the tire models of Section 6. The resulting simulation code is modular in the sense that the dynamic equations, the suspensions and the axle load balance equations, and the tire model equations are separated. This makes it easy to substitute one of these sub-models for another. The organization of the resulting Simulink model is illustrated in Appendix B. In the present implementation the chassis dynamics, suspension and axle load balance equations, and wheel/tire models are implemented as separate S-functions in Simulink. This is not the optimal implementation structure for simulation-speed performance, but results in a well organized code that is easy to overview.

The implemented vehicle configuration is a 4x2 tractor-semitrailer. The semitrailer has three axles. The model includes wheel rotational dynamics with torque inputs, but may also be used without wheel dynamics with longitudinal slips as direct inputs. The wheel torques $M_{w,i}$ or the longitudinal slips λ_i with $i \in \{fl, fr, rl, rr, s1l, s1r, s2l, s2r, s3l, s3r\}$, and the front wheel steering angle δ are the inputs to the model. Wind-drag forces are not included in the implementation. The parameters of the model are listed in Table 2.

Variable road-surface conditions are easily modeled by providing an adhesion reduction factor as a lookup-table in position xy-coordinates.

The mass distribution of the tractor and semitrailer sprung bodies were modeled as combinations of rectangular boxes with homogeneous density. This makes it ease to arrive at desired inertia properties. See Appendix C.

A 3D-animation routine has been developed to illustrate simulation results. This routine is based on standard Matlab graphics, and produce output as shown in Figure 10.

8.1 Real-Time Performance

Application of the present model in real-time simulation has been considered. For this reason all nonlinear algebraic equations have been avoided. Such equations would otherwise result in algebraic loops that require iterative solution algorithms. With such algorithms it is difficult to obtain guaranteed convergence time, which makes it difficult to guarantee real-time performance. The present model have a deterministic number of floating-point operations at each simulation step (for fixed time-step integration methods). This prerequisite for a real-time simulation model is therefore fulfilled.

The present implementation does not simulate in real-time. The simulation speed is around on tenth of real-time for variable-step Simulink solver ode45 Dormand-Prince on a standard Pentium II PC running at 366 MHz. There are several possible reasons for this:

1. The number of floating point operations is too large in each step.

2. The implementation code-structure is inefficient.

3. The model contains stiff modes forcing the solver to use small steps.

Chassis	
m_{ts}	Tractor sprung mass
m_{ss}	Semitrailer sprung mass
$\bar{r}_{CG,ts}$	Tractor sprung body CM location
$\bar{r}_{CG,ss}$	Semitrailer sprung body CM location
$\underline{I}_{ts}$	Tractor sprung body inertia matrix
$\underline{I}_{ss}$	Semitrailer sprung body inertia matrix
C_c	Tractor frame torsional stiffness

*Axles and suspensions**[*]	
$\bar{r}_{w,l}$	Left wheel location
$\bar{r}_{w,r}$	Right wheel location
$\bar{r}_{s,l}$	Left suspension location
$\bar{r}_{s,r}$	Right suspension location
C_s	Suspension vertical stiffness
D_s	Suspension vertical damping coefficient
C_r	Roll-bar stiffness
h_s	Unloaded suspension length.

*Wheel and tires**[*]	
R_w	Wheel radius
$C_\lambda{}^{[†]}$	Tire longitudinal stiffness
$C_\alpha{}^{[†]}$	Tire cornering stiffness
$f : \lambda \mapsto \mu_x{}^{[‡]}$	Longitudinal adhesion coefficient mapping at pure braking (lookup-table)
$g : \alpha \mapsto \mu_y{}^{[‡]}$	Lateral adhesion coefficient mapping at pure cornering (lookup-table)

Table 2 Model parameters.

The first reason is less likely. Even if there are many floating-point operations to compute in the model, those are very fast to execute. Matlab has very efficient numerics using BLAS/LAPACK. The second reason is definitively an issue. The code has been structured for user simplicity rather than optimal performance. In particular the partitioning of the model on many S-functions is inefficient. Collecting everything in one S-function would bring down the number of S-function calls by a magnitude. The possibility to implement this S-function in C should probably also be considered. The third reason in the list may also be an issue. There are indications that the parameters used in the validation simulations lead to fast modes. During transient behaviour the variable-step solver bring down the step-length to very small values. Efforts are needed to eliminate any stiff behaviour.

9. Validation

Experimental data for a 4x2 tractor-semitrailer vehicle recorded on a test-track was kindly provided by Volvo Truck Corporation, together with some data on the vehicle[‡]. The experiments were designed for other purposes than the validation of the present model, and were performed before the work on this model started. A set of model parameters corresponding to the tested vehicle was derived. Since the provided data did not cover the complete set of parameters of the model, some assumptions were made. In particular it is difficult to determine tire data and suspension data with high accuracy. The provided tire data did not give enough information for the slip-circle model. Therefore a linear tire model was used in the validation. No information except from approximate mass and dimensions was provided on the semitrailer parameters. Nonlinear lookup-table mappings for the damper characteristics were provided, and was included in the model. Most of the 31 test-scenarios only included steering actions. The steering actions were of moderate magnitude, in the sense that they only generate small lateral slips. Therefore the linear tyre model used in the validation simulations is probably quite accurate. Some scenarios seem to include braking actions in combination with the steering. Unfortunately, no information on how the braking was applied was provided, which makes it difficult to use the data for validation.

The recorded variables of interest were: front wheel angles, vehicle speed, kingpin-angle, yaw-rate, and suspension travel for the four corners of the tractor. The average of the left and right front wheels angles were used as inputs to the model.

The linear constant speed 4-DOF dynamic tractor-semitrailer model derived in [Gäf01] was tuned with parameters corresponding to those of the 9-DOF model. This 4-DOF model has the lateral velocity V, yaw-rate r, articulation angular rate $\dot{\psi}$, and articulation angle ψ as state variables.

Both the 4-DOF and the 9-DOF models were simulated with the average front steering angle of the experimental data as inputs. Results from a choice of scenarios are presented in Appendix D. The 4-DOF model only reproduces the kingpin-angle and the yaw-rate.

9.1 Lane-Change Maneuver

Appendices D.1 and D.2 shows the typical results from two lane-change maneuvers. Both models show good accordance with experimental data with respect to kingpin-angle and yaw-rate. The kingpin-angle peaks are a bit too large on the models. The suspension travel of the 9-DOF model is well reproduced on the rear axle, but significantly smaller on the front axle.

9.2 Step-Steering Maneuver

Appendices D.3 and D.4 shows the typical results from two step-steering maneuvers. The results are similar to those of the lane-change maneuvers. The models performs well. An overshoot in the articulation angle is present

---

[‡]The detailed data on the vehicle tests are classified corporate information.
[*]One set of parameters for each instance of the object class.
[†]For linear tire model.
[‡]For slip-circle tire model.

in the model results for the first maneuver, but absent in the second. The reason for this is difficult to understand without more information on the experimental setup.

9.3 Random Steering Maneuvers

Appendix D.5 shows the results from random-steering maneuvers. The results are similar to those of the previous maneuvers. One can note that the longitudinal speed decreases slightly during the maneuvers for the 9-DOF model. This is because the experiments were performed under cruising conditions, while the model simulates a free-rolling scenario. The energy loss in the front tires during steering then reduces the speed. The overshoots in the kingpin-angle are still present. There are also some discrepancies in the reproduction of the yaw-rate in this scenario. The reproduction of the rear axle suspension travel is good.

9.4 Comments on the Results

Some re-tuning of parameters were performed to improve the validation results. Still several of the parameters are uncertain, and would require more accurate values to obtain optimal results. It was noted that the tire parameters have large impact on the reproduction of the king-pin angle and the yaw-rate. The discrepancies in the front suspension travel may partly be explained by uncertainty in the position of the suspension travel sensors.

The motivation for using the 9-DOF model instead of the simpler 4-DOF model is the inclusion of the tire normal forces. Those forces were not measured in the experiments, but they correspond to the suspension travel. Since the suspension travel is reasonable well reproduced by the 9-DOF model it is concluded that the tire normal forces are equally well reproduced. In the present scenarios the linear model performs equally well compared to the 9-DOF model with respect to kingpin-angle and yaw-rate. Hence good reproduction of normal forces are not needed to reproduce the planar behaviour of these scenarios. Still it expected that the load transfer will have significant influence in the case of unilateral braking actions, which may be applied by yaw-stabilization systems. To really validate the benefits of good normal-force modeling more aggressive scenarios are needed, where the load-transfer is significant and the tires operate in the nonlinear region. Experiments with combined braking and cornering would probably also require more accurate models because of additional load-transfer. Experiments with "large" state-variable registerings, where the linear model is less accurate, would also be interesting to investigate to evaluate possible advantages of using the nonlinear model. This could also include experiments on slippery surfaces with little adhesion.

To conclude, the validation results seem reasonable considering the uncertainties in the parameters. Qualitatively the performance seems realistic.

10. Simulations

In appendix E the output from two lane-change maneuvers are presented. In these simulations the slip-circle model is used. The first simulation
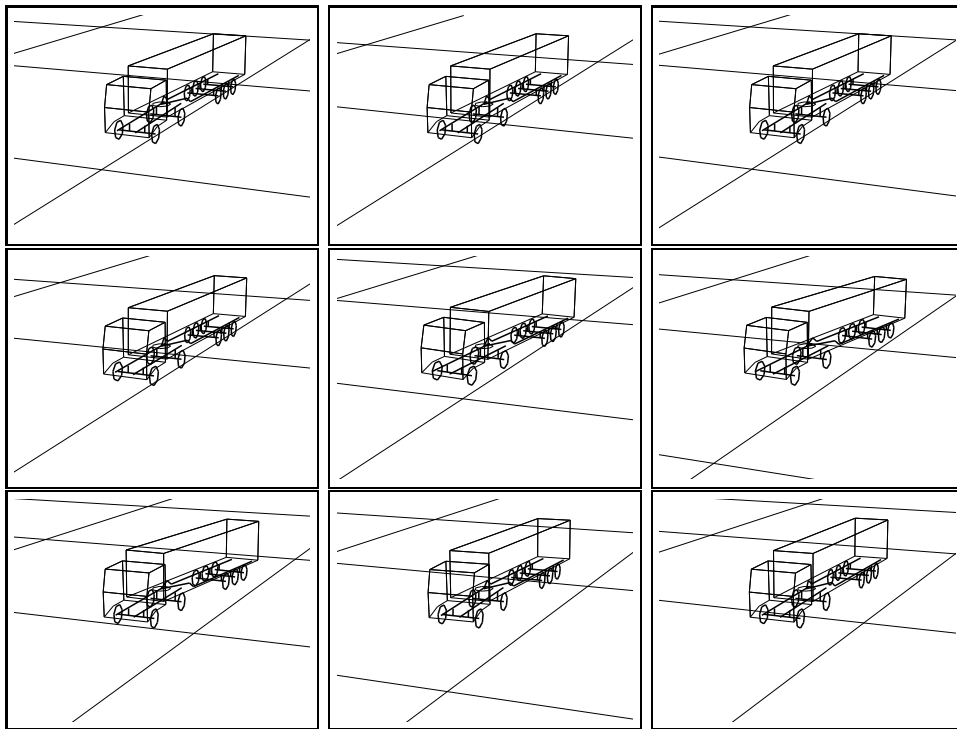
Figure 10 Matlab 3D-animation of the vehicle.

shows a free-rolling violent lane-change maneuver. Wheel normal forces are just above zero in the critical part of the maneuver. In the second maneuver the tractor rear wheel are locked with full braking. Not surprisingly this leads to a jack-knifing accident. Note that some tire normal forces become zero at certain time intervals. The method described in Section 5.4 for roll-over conditions is not used in these simulations. The normal forces are simply limited to be positive. This will of course reduce the validity of the model when the limits are hit. This simulation is intended to show a clearly nonlinear behaviour of the model. The plots are merely examples of some of the outputs that may be extracted from the simulations.

11. Future Work

Work is initiated on including unsprung masses in the equations of motion. Real-time optimizations in line with the discussion of Section 8.1 should be done to speed up simulations. Further validation is needed to investigate the ability of the model to reproduce correct nonlinear behaviour.

12. Conclusions

A nonlinear dynamic 9-DOF tractor-semitrailer model has been presented. Validation of the model indicates that load-transfer is accurately modeled. This implies that the model may give realistic results in simulation of handling maneuvers near and beyond the adhesion limits. Hence the model can be suitable for studies on advanced chassis control in handling-maneuvers.

13. Acknowledgements

14. References

[CGS00] V. Claesson, M. Gäfvert, and M. Sanfridson. Proposal for a distributed computer control system in a heavy-duty truck. Technical Report No. 00-16, Department of Computer Engineering, Chalmers Univ. of Technology, 2000. DICOSMOS Report.

[CT95] Chieh Chen and Masayoshi Tomizuka. Dynamic modeling of articulated vehicles for automated highway systems. In *Proceedings of the American Control Conference*, pages pp. 653 – 657, Seattle, USA, 1995.

[CT00] Chieh Chen and Masayoshi Tomizuka. Lateral control of commercial heavy vehicles. *Vehicle System Dynamics*, (33):391–420, 2000.

[DYT00] J. D. Demerly and K. Youcef-Toumi. Non-linear analysis of vehicle dynamics (NAVDyn): A reduced order model for vehicle handling analysis. Technical report, SAE Paper 2000-01-1621, 2000.

[Edl91] S. Edlund. Tyre models: Subreport –91. Technical report, Volvo Truck Corporation, 1991. (classified).

[Ell69] John Ronaine Ellis. *Vehicle Dynamics*. Business Books Ltd., London, 1969.

[Ell88] John R. Ellis. *Road Vehicle Dynamics*. John R. Ellis Inc, 1988.

[Ell94] J.R. Ellis. *Vehicle Handling Dynamics*. Mechanical Engineering Publications Limited, London, 1994.

[FC93] Grant R. Fowles and George L. Cassiday. *Analytical Mechanics*. Saunders College Publishing, 5 edition, 1993.

[Gäf01] M. Gäfvert. Studies on yaw-control of heavy-duty trucks using unilateral braking. Technical Report ISRN LUTFD2/TFRT–7598–SE, Department of Automatic Control, Lund Institute of Technology, Sweden, 2001. DICOSMOS Report.

[GSC00] M. Gäfvert, M. Sanfridsson, and V. Claesson. Truck model for yaw and roll dynamics control. Technical Report ISRN LUTFD2/TFRT–7588–SE, Department of Automatic Control, Lund Institute of Technology, 2000. DICOSMOS Report.

[KN00] U. Kiencke and L. Nielsen. *Automotive Control Systems*. Springer, 2000.

[Leu70] Philip M. Leucht. The directional dynamics of the commercial tractor-semitrailer vehicle during braking. Technical Report SAE Paper 700371, Society of Automotive Engineers, 1970.

[LU84] P. Lidström and U. Uhlhorn. Teknisk mekanik 2f. Avdelningen för Mekanik, Lunds Tekniska Högskola, 1984. (In Swedish).

[Mik68] E. C. Mikulcik. *The dynamics of Tractor-Semitrailer Vehicles: The Jackknifing Problem*. PhD thesis, Cornell University, 1968.

[Mik71] E. C. Mikulcik. The dynamics of tractor-semitrailer vehicles: The jackknifing problem. Technical Report SAE Paper No. 710045, Society of Automotive Engineers, 1971.

[RA95]   R. Ranganathan and A. Aia. Development of heavy vehicle dynamic stability analysis model using MATLAB/SIMULINK. Technical report, SAE Paper 952638, 1995.

[Say92]   M. W. Sayers. Computer modeling and simulation of vehicle dynamics. *UMTRI Research Review*, 23(1):1–15, 1992.

[SCG00]   M. Sanfridson, V. Claesson, and M. Gäfvert. Investigation and requirements of a computer control system in a heavy-duty truck. Technical Report TRITA-MMK 2000:5, ISSN 1400-1179, ISRN KTH/MMK–00/5–SE, Mechatronics Lab, Department of Machine Design, Royal Institute of Technology, 2000. DICOSMOS Report.

[SPP96]   D. J. Schuring, W. Pelz, and M. G. Pottinger. A model for combined tire cornering and braking forces. Technical report, SAE Paper 960180, 1996.

A. Nomenclature

Body configuration and reference systems	
$\mathcal{B}_{tu}$	Tractor unsprung body
$\mathcal{B}_{su}$	Semitrailer unsprung body
$\mathcal{B}_{ts}$	Tractor sprung body
$\mathcal{B}_{ss}$	Semitrailer sprung body
$\mathcal{B}_h$	Hitch (tractor rear part) body
S_{tu}	Tractor reference system attached to $\mathcal{B}_{tu}$
S_{su}	Semitrailer reference system attached to $\mathcal{B}_{su}$
S_{ts}	Tractor reference system attached to $\mathcal{B}_{ts}$
S_{ss}	Semitrailer reference system attached to $\mathcal{B}_{ss}$
S_h	Hitch wheel reference system attached to $\mathcal{B}_h$
O	Origin for S_{tu}, S_{su}, S_{ts}, S_{ss}, S_h

Indices	
tu	Tractor unsprung
su	Semitrailer unsprung
ts	Tractor sprung
ss	Semitrailer sprung
h	Hitch
f	Front axle
r	Rear axle
s	Semitrailer axle
l	Left side
r	Right side

Geometry	
$\bar{r}_{CM,ts}$	Center of mass location for $\mathcal{B}_{ts}$
$\bar{r}_{CM,ss}$	Center of mass location for $\mathcal{B}_{ss}$
$\bar{r}_{s,i,j}$	Location of suspension at side j on axle i
$\bar{r}_{w,i,j}$	Location of wheel at side j on axle i

Kinematics

$\bar{v}_O$	velocity of O expressed in S_{tu}
U	Longitudinal component of v_O
V	Lateral component of v_O
W	Vertical component of v_O
$\bar{\omega}_{tu}$	Angular velocity of S_{tu}
r	Yaw velocity of S_{tu}
$\bar{\omega}_{su}$	Angular velocity of S_{su}
r'	Yaw velocity of S_{su}
ψ	Articulation angle (angle between S_{tu} and S_{su})
χ_t	Tractor pitch angle
ϕ_t	Tractor roll angle
χ_s	Semitrailer pitch angle
ϕ_s	Semitrailer roll angle
ϕ_h	Hitch body roll angle
$\underline{R}^{tu}_{ts}$	Coordinate transformation matrix from S_{ts} to S_{tu}
$\underline{R}^{su}_{ss}$	Coordinate transformation matrix from S_{ss} to S_{su}
$\underline{R}^{tu}_{h}$	Coordinate transformation matrix from S_h to S_{tu}
$\underline{R}^{su}_{tu}$	Coordinate transformation matrix from S_{su} to S_{tu}

Kinetics

m_{ts}	Tractor mass ($\mathcal{B}_{ts}$)
m_{ss}	Semitrailer mass ($\mathcal{B}_{ss}$)
$\underline{I}_{ts}$	Tractor inertial tensor with respect to O
$\underline{I}_{ss}$	Semitrailer inertial tensor with respect to O
$\bar{F}'_{ts}$	Internal force between $\mathcal{B}_{ts}$ and $\mathcal{B}_h$
$\bar{M}'_{ts}$	Internal moment between $\mathcal{B}_{ts}$ and $\mathcal{B}_h$
$\bar{F}_{ss}$	Internal force between $\mathcal{B}_{ss}$ and $\mathcal{B}_h$
$\bar{M}'_{ss}$	Internal moment between $\mathcal{B}_{ss}$ and $\mathcal{B}_h$
$\bar{F}_{ts}$	Sum of external forces acting on $\mathcal{B}_{ts}$
$\bar{M}_{ts}$	Sum of external moments acting on $\mathcal{B}_{ts}$
$\bar{F}_{ss}$	Sum of external forces acting on $\mathcal{B}_{ss}$
$\bar{M}_{ss}$	Sum of external moments acting on $\mathcal{B}_{ss}$
$\bar{F}_{s,i,j}$	Suspension force at side j on axle i.
$\bar{F}_{w,i,j}$	Tire-road contact force at wheel on side j of axle i

B. Simulink Model
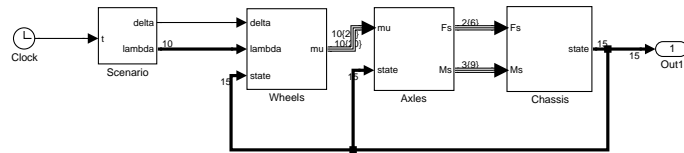
Figure 11   Top level view of Simulink model
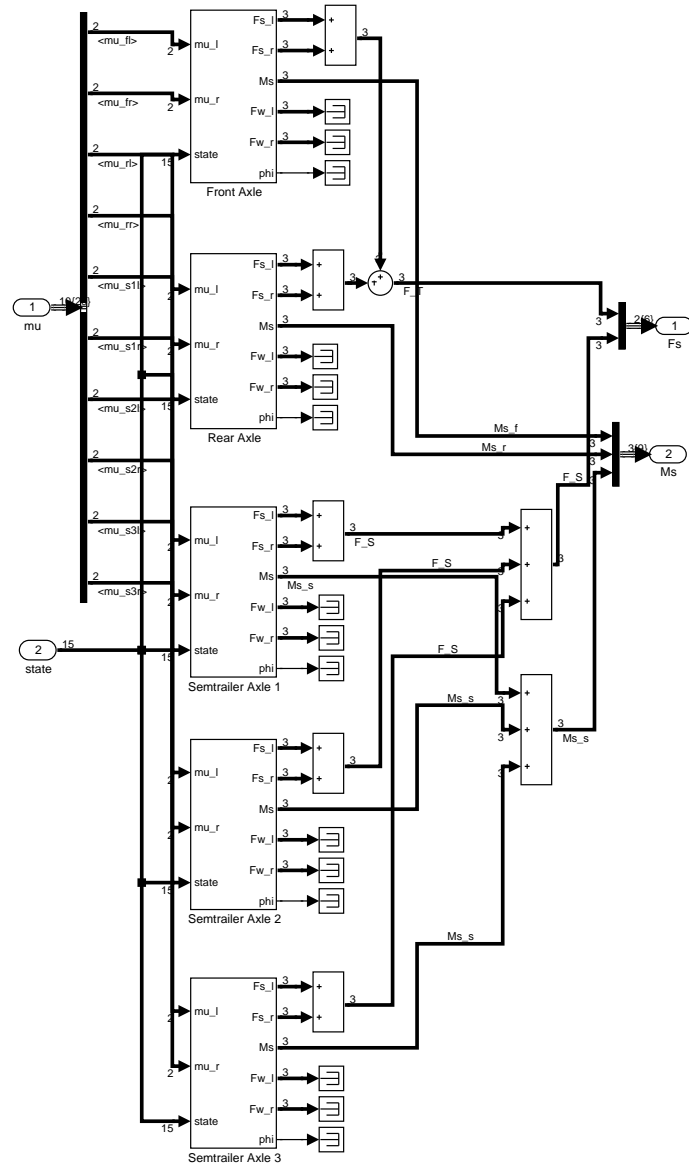
Figure 12   Axles block view of Simulink model
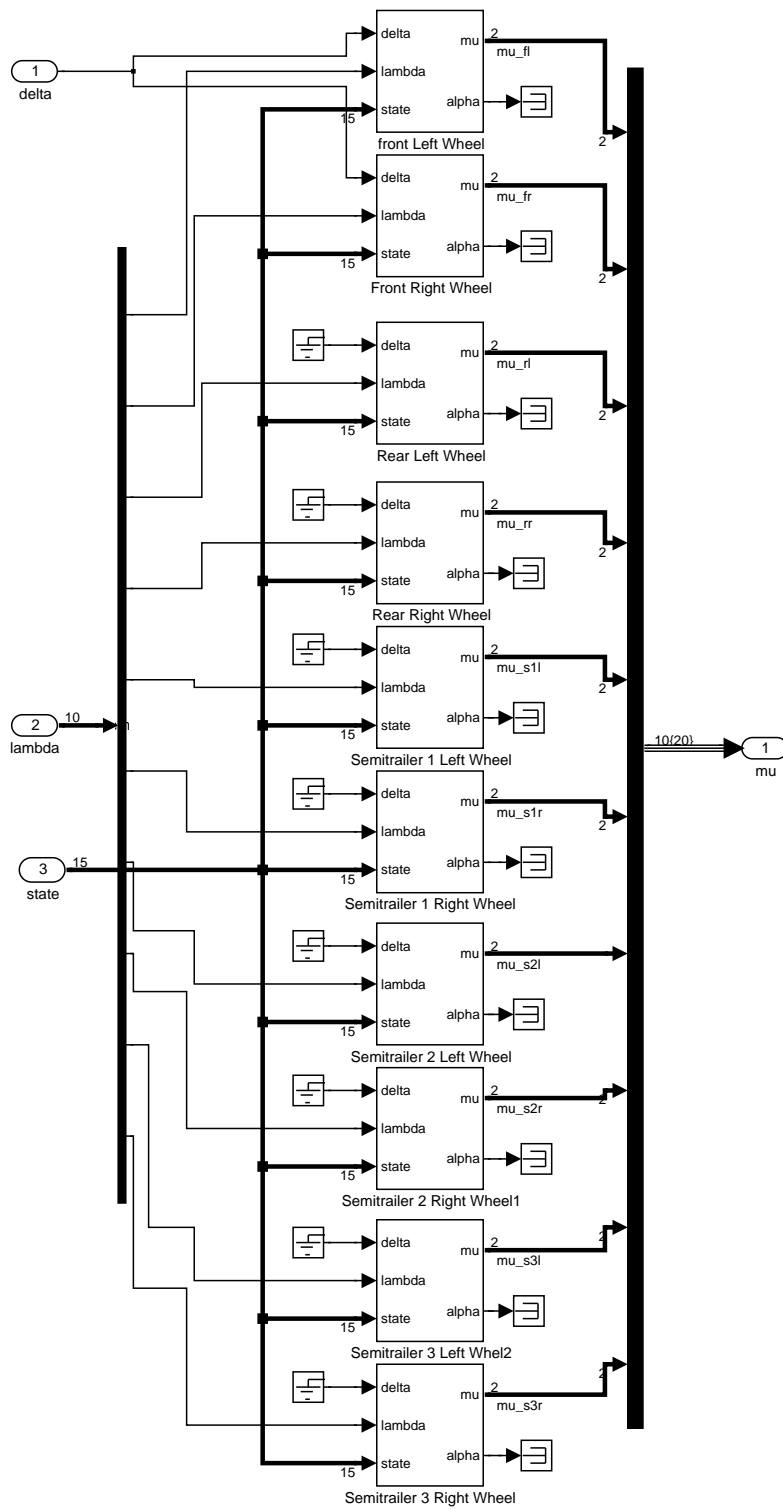
Figure 13 Wheels block view of Simulink model

C. Moments of inertia

It is convenient to consider the body mass distribution as combinations of rectangular blocks with homogeneous density. This makes it easy to compute the moments of inertia for the complete chassis body with respect to a certain origin and a certain coordinate system aligned with the block. Since the moments of inertia are additive, the resulting moments of inertia for the body are the sum of the moments of inertia for the blocks. Recall that the inertia terms occurring in the model equations are $I_{ij} = \int r_i r_j dm_P$ with $i, j \in \{x, y, z\}$, instead of the traditional terms defined as the elements of the matrix $\int \left(\bar{r}_P^T \bar{r}_P \underline{1} - \bar{r}_P \bar{r}_P^T \right) dm_P$.

Now regard a homogeneous rectangular block of mass m with the sides A, B, C in the $\bar{e}_x, \bar{e}_y, \bar{e}_z$ directions respectively. The position vector of the cg of the block with respect to O is $\bar{r}_{cg} = R_x \bar{e}_x + R_y \bar{e}_y + R_z \bar{e}_z$. Then

$$
\begin{aligned}
I_{xx} &= m \left(R_x^2 + \tfrac{A^2}{12} \right) & I_{xy} &= m R_x R_y & I_{xz} &= m R_x R_z \\
I_{yx} &= I_{xy} & I_{yy} &= m \left(R_y^2 + \tfrac{B^2}{12} \right) & I_{yz} &= m R_y R_z \\
I_{zx} &= I_{xz} & I_{zy} &= I_{yz} & I_{zz} &= m \left(R_z^2 + \tfrac{C^2}{12} \right)
\end{aligned}
\tag{59}
$$

D. Validation Results

D.1 Lane-change maneuver (i)
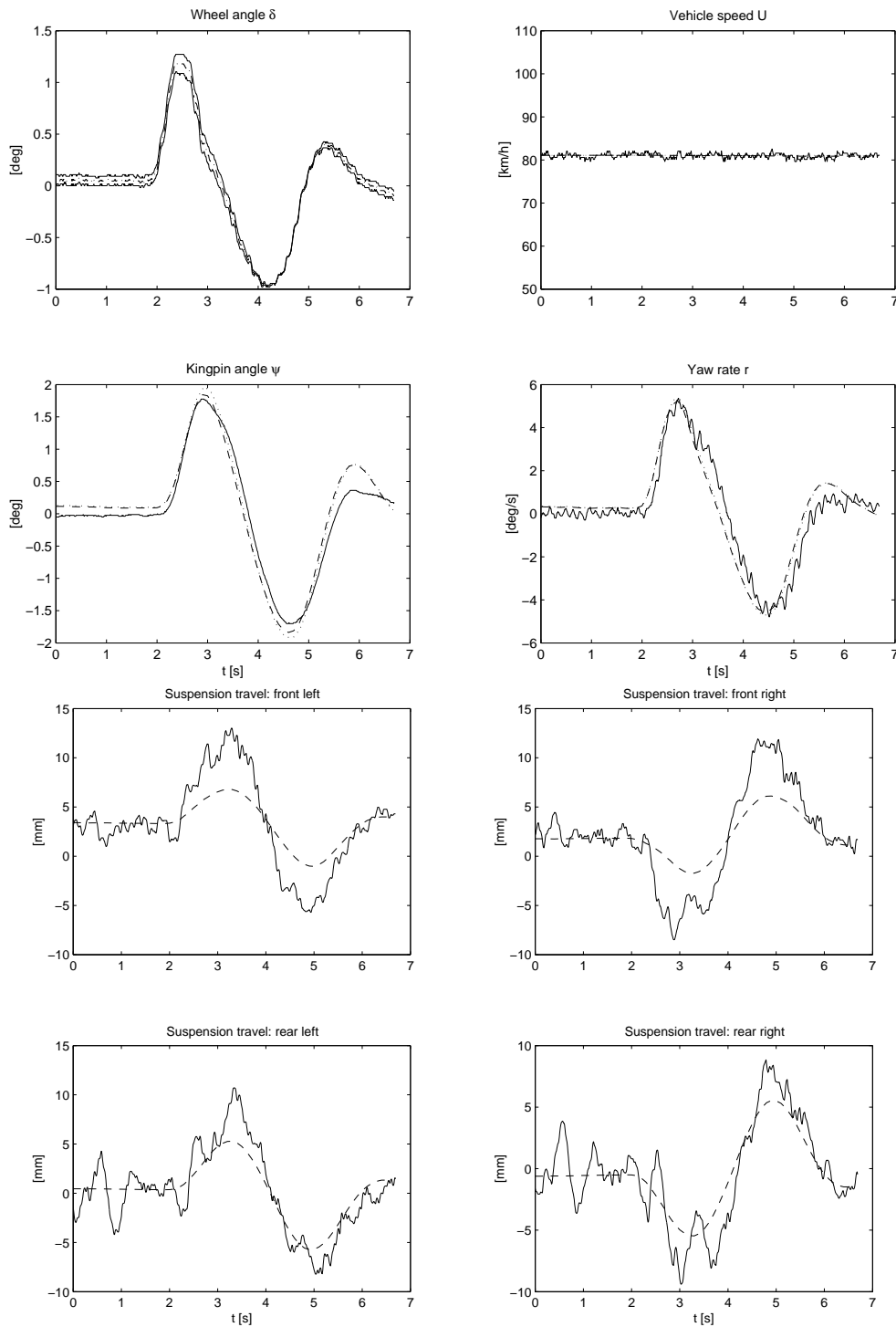
Figure 14 Solid: Experiment; Dashed: 9-DOF model; Dotted: Linear 4-DOF model

D.2 Lane-change maneuver (ii)
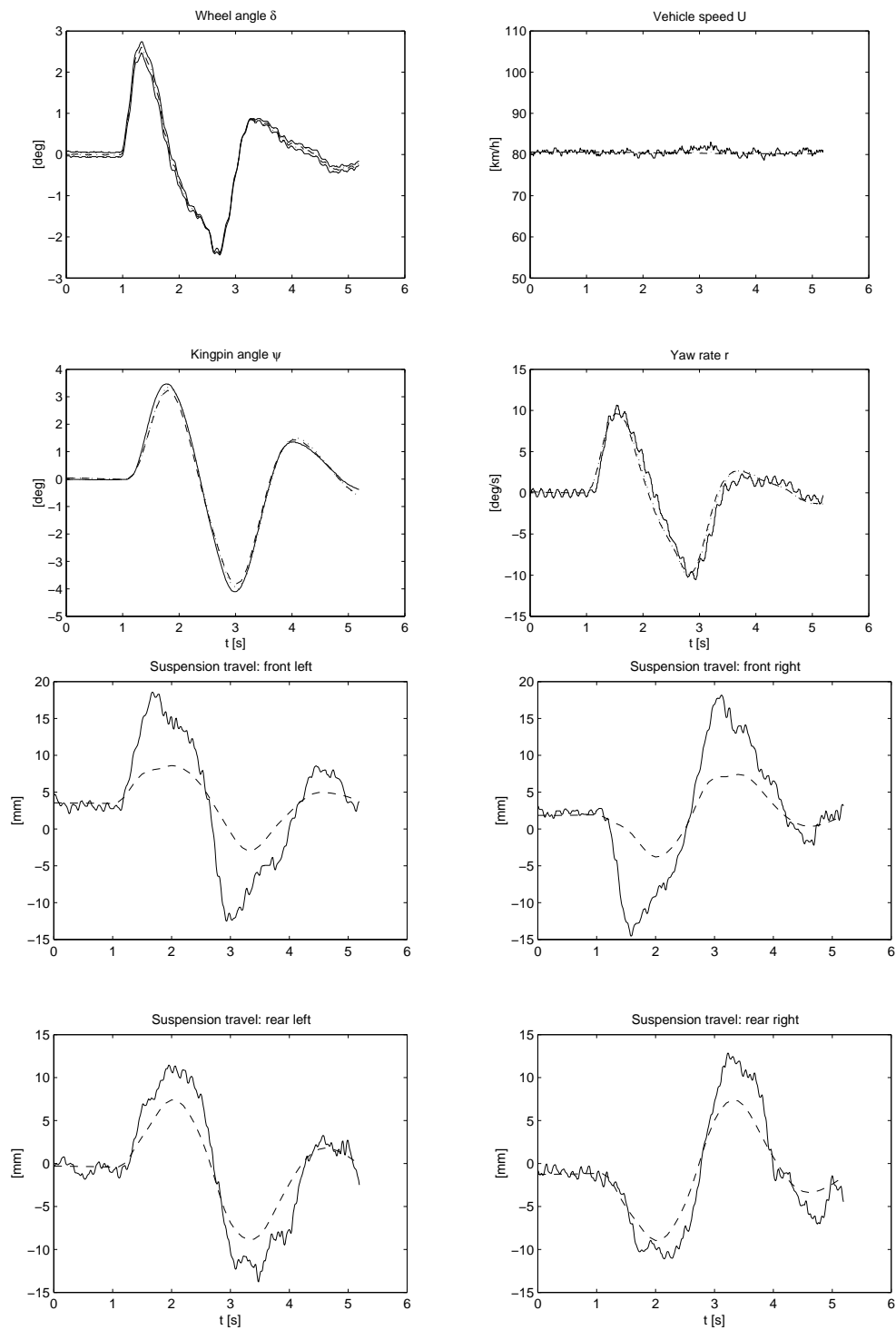
Figure 15 Solid: Experiment; Dashed: 9-DOF model; Dotted: Linear 4-DOF model

D.3 Step-steering maneuver (i)
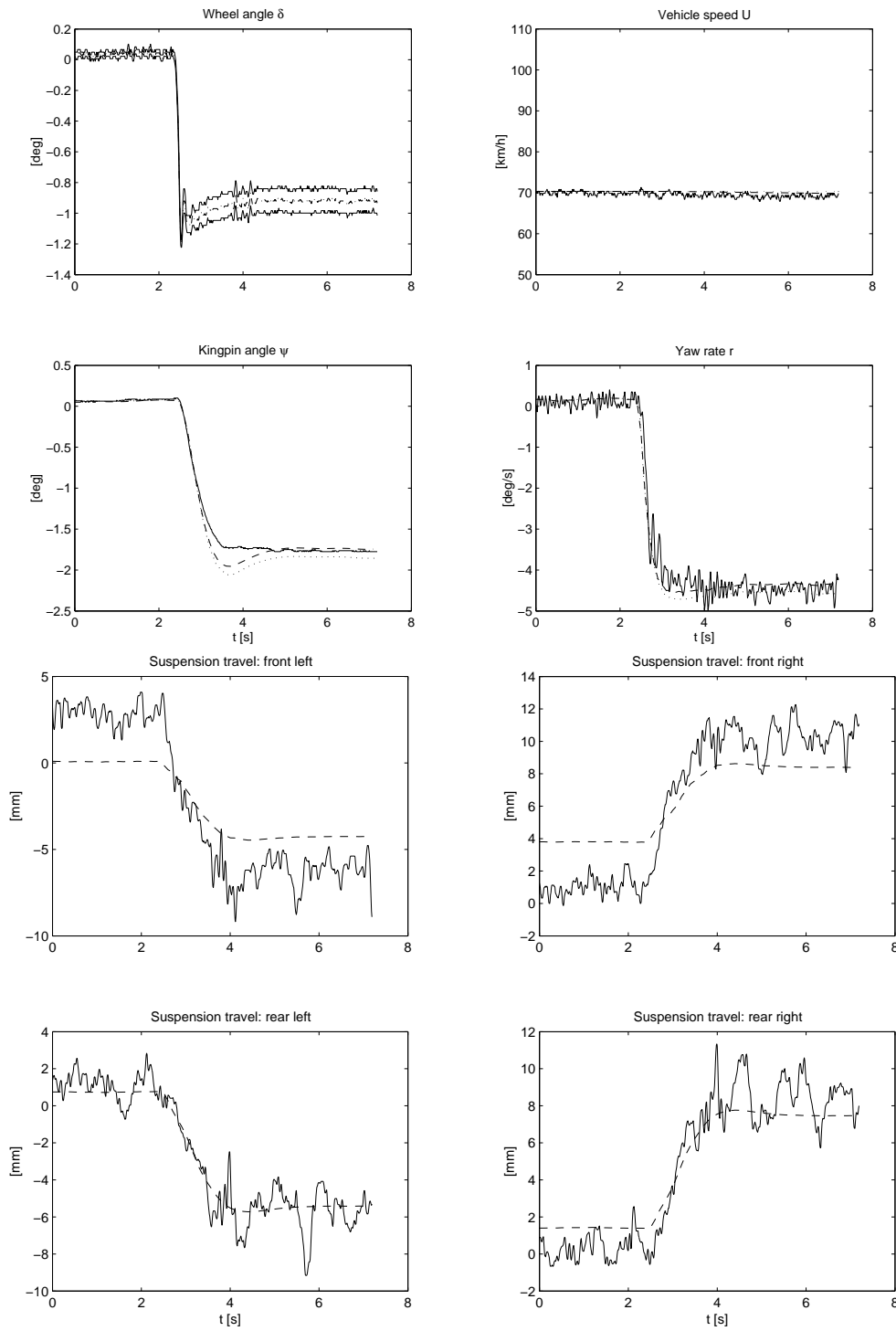
Figure 16 Solid: Experiment; Dashed: 9-DOF model; Dotted: Linear 4-DOF model
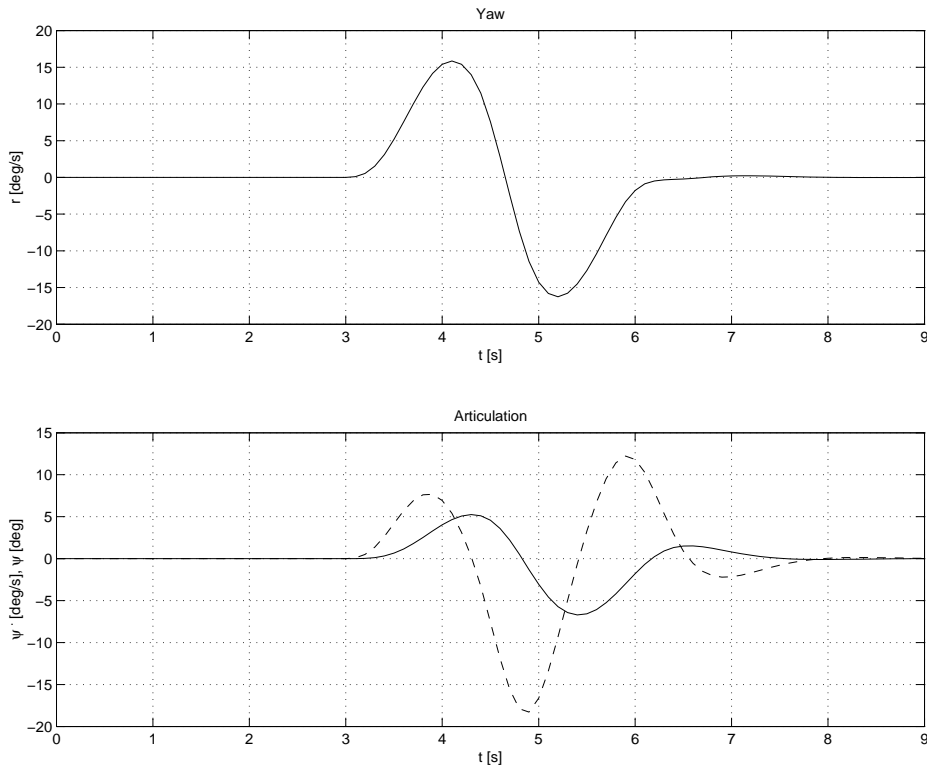
D.4 Step-steering maneuver (ii)
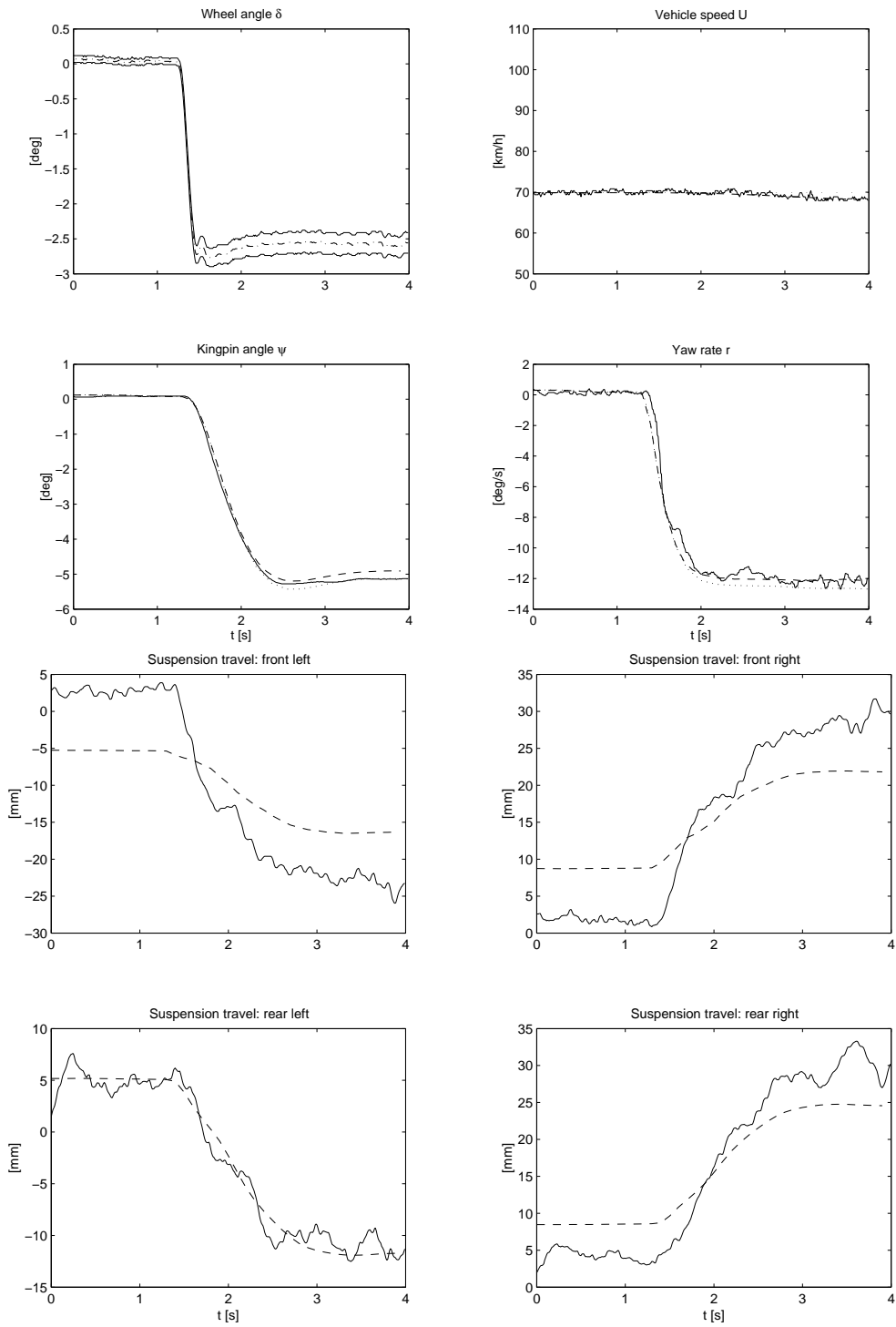
Figure 17 Solid: Experiment; Dashed: 9-DOF model; Dotted: Linear 4-DOF model

D.5 Random steering maneuvers
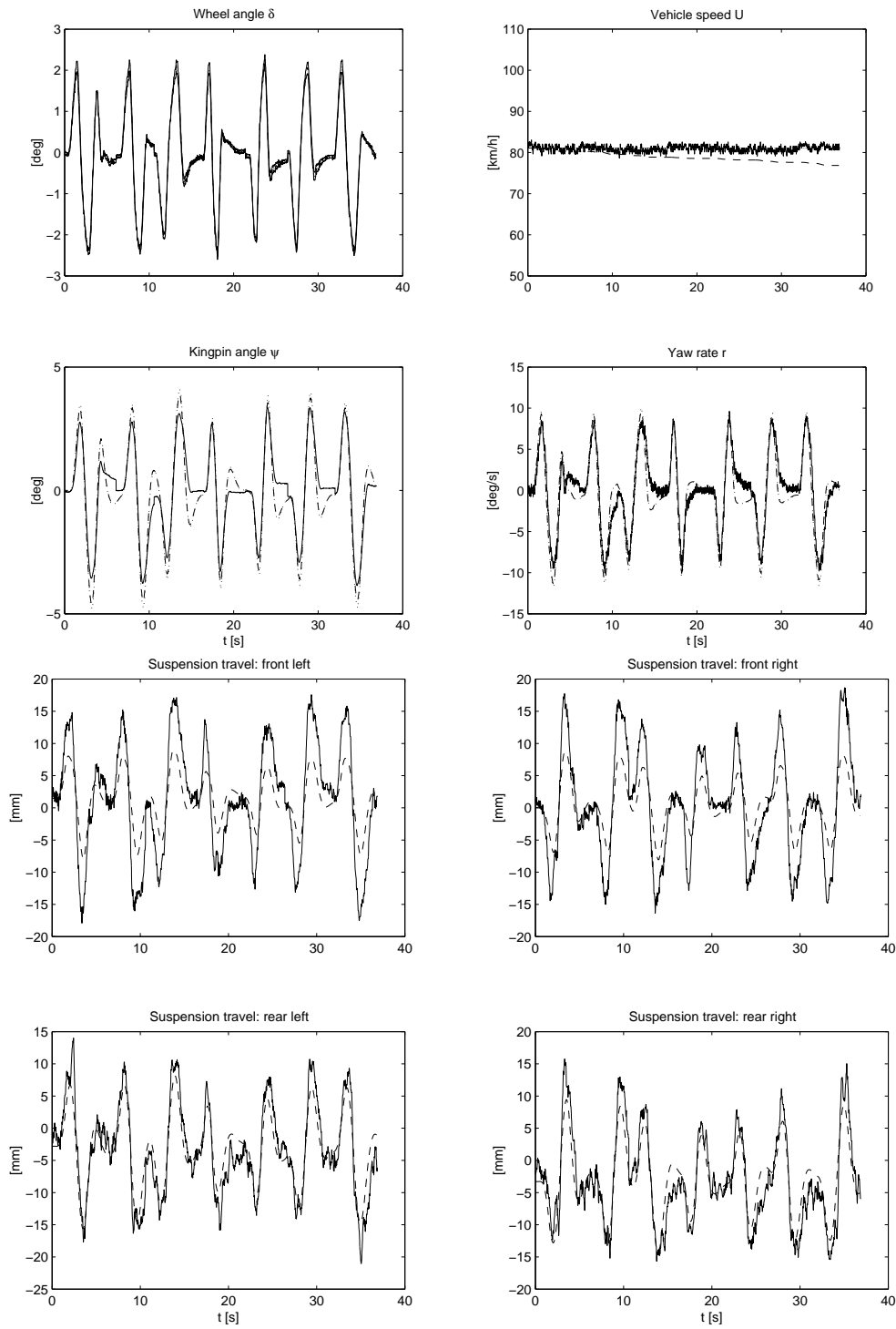
**Figure 18** Solid: Experiment; Dashed: 9-DOF model; Dotted: Linear 4-DOF model

40

E. Simulation Results

E.1 Lane-Change Maneuver
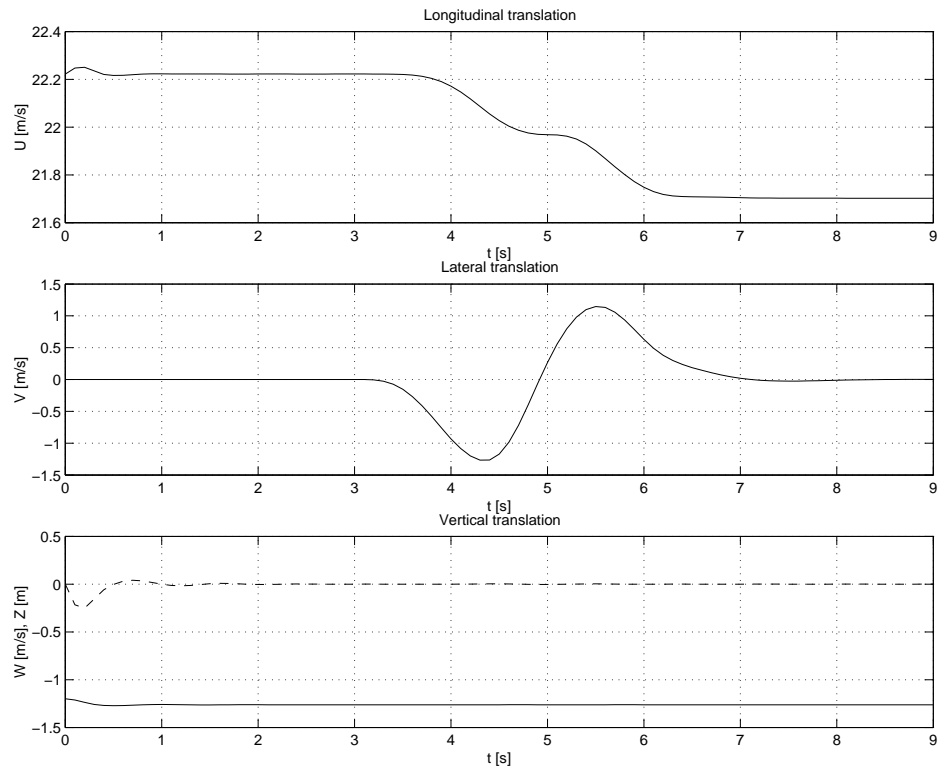
Figure 19 Longitudinal, lateral, and heave motion. (Solid: position; Dashed: velocity)

Figure 20   Yaw motion. (Solid: position; Dashed: velocity)
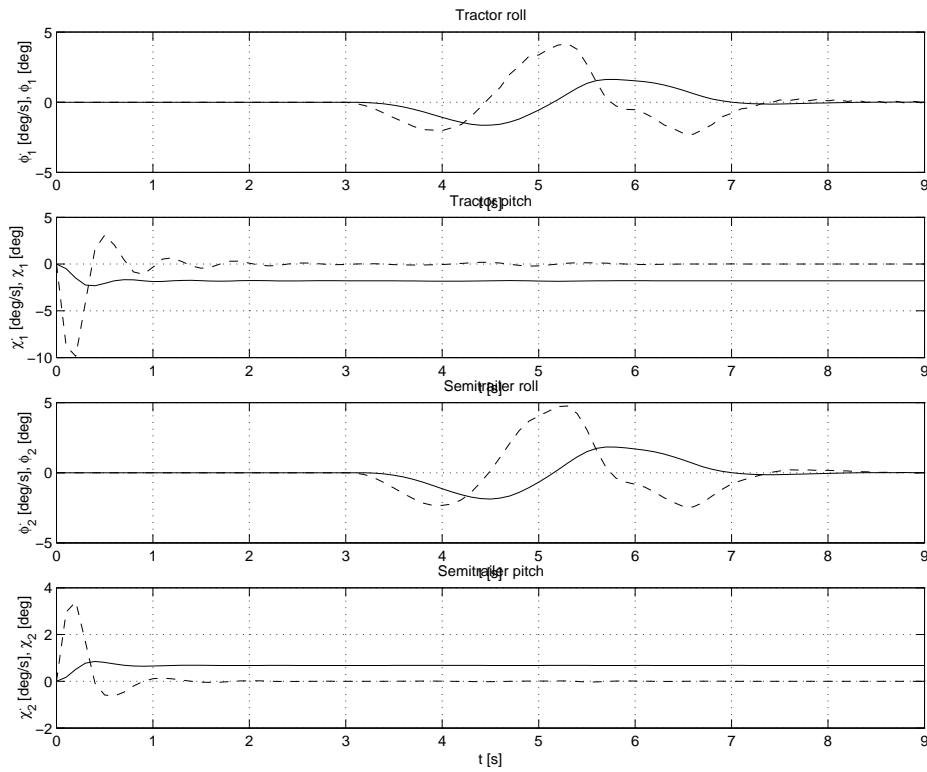
Figure 21   Roll and pitch motion. (Solid: position; Dashed: velocity)

42
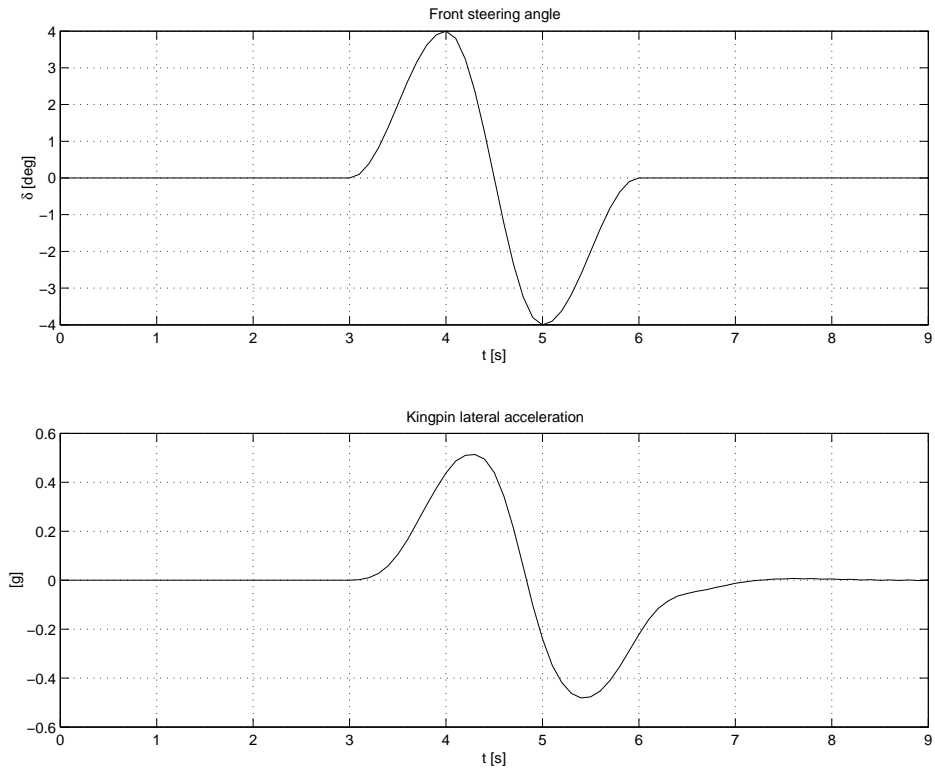
Figure 22 Steering input and lateral acceleration at kingpin.
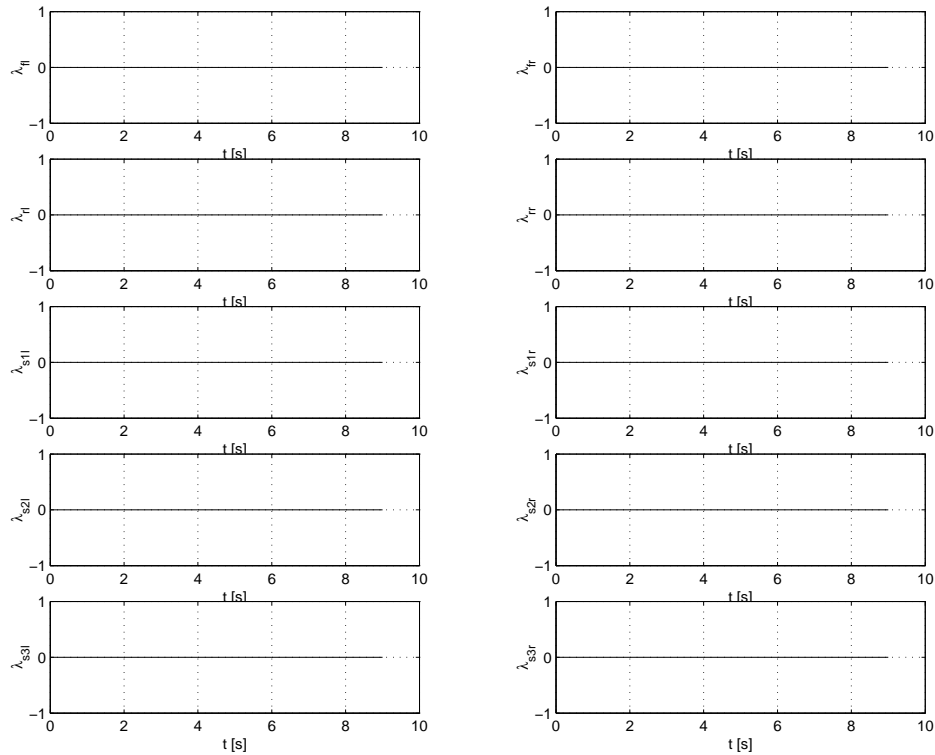
Figure 23 Longitudinal slip inputs. (Zero since no braking is applied.)

43
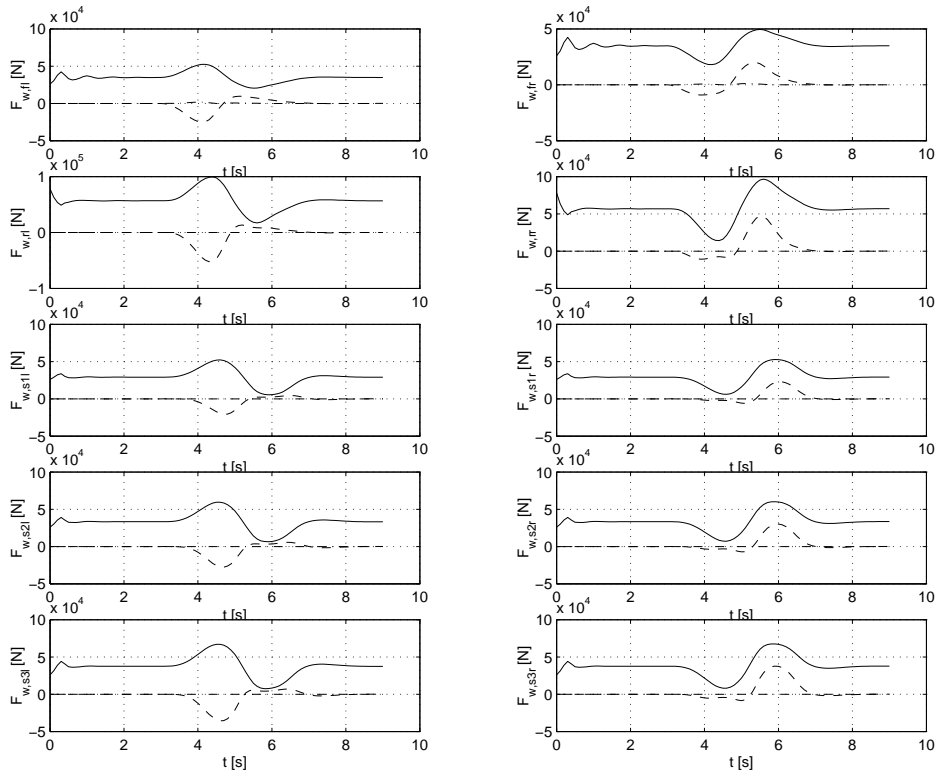
Figure 24 Tire forces in tractor and semitrailer unsprung reference systems respectively. (Dash-dotted: longitudinal; Dashed: lateral; Solid: vertical)
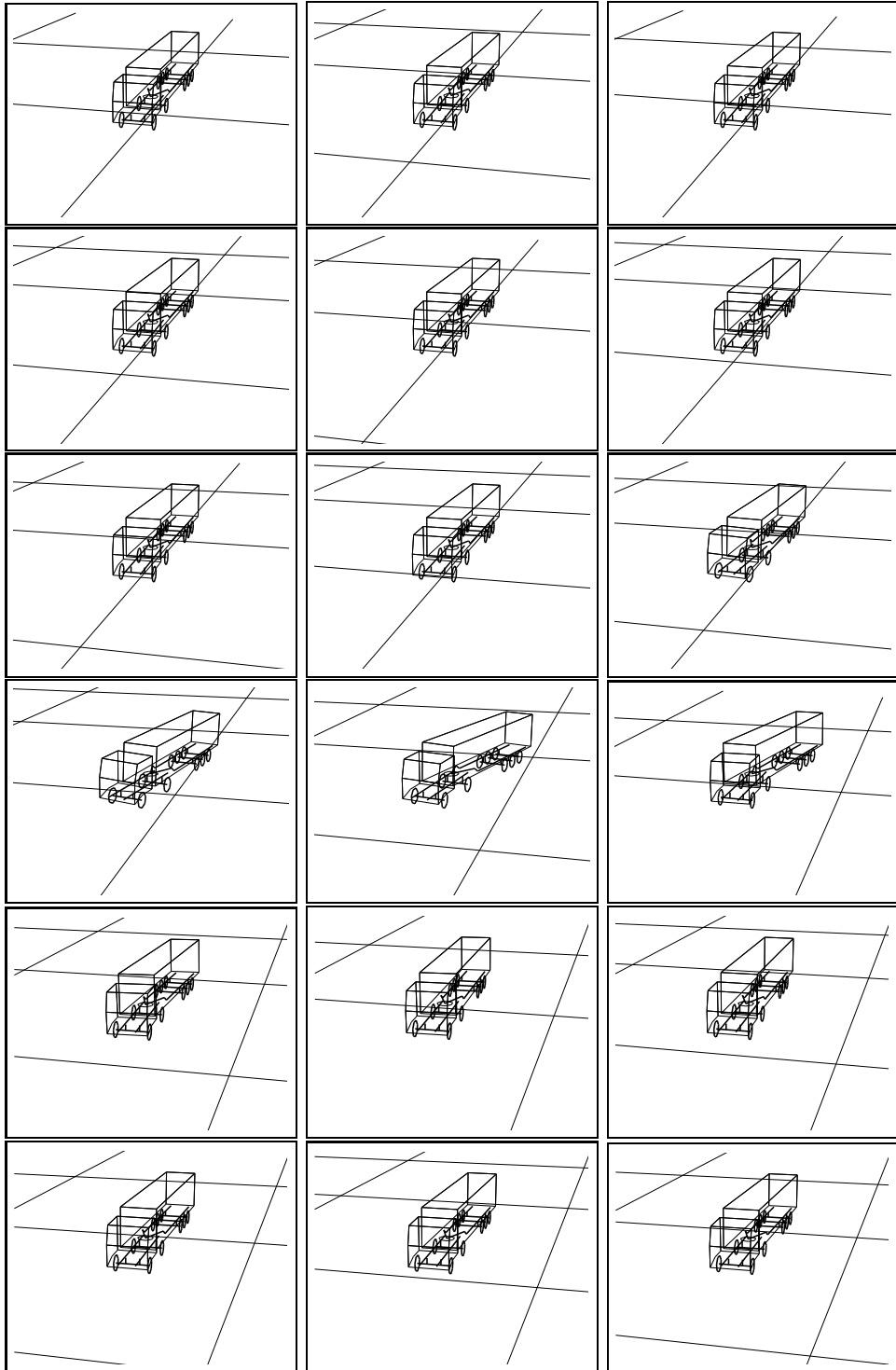
Figure 25 Matlab 3D-animation of the vehicle.

E.2 Lane-Change Maneuver with Jack-knifing
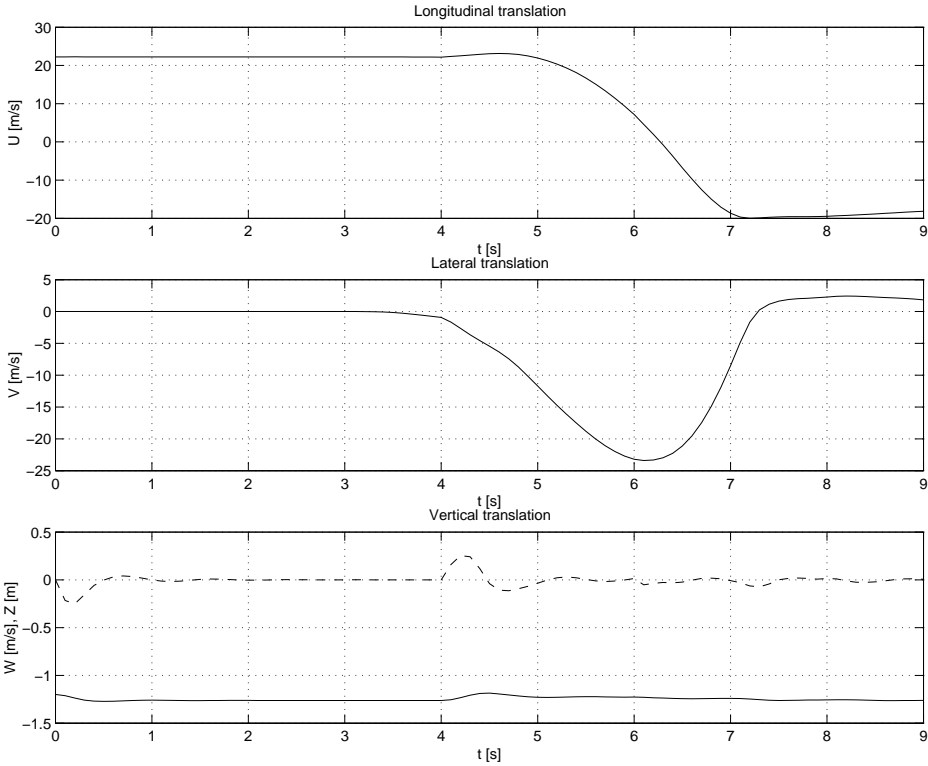
Figure 26 Longitudinal, lateral, and heave motion. (Solid: position; Dashed: velocity)
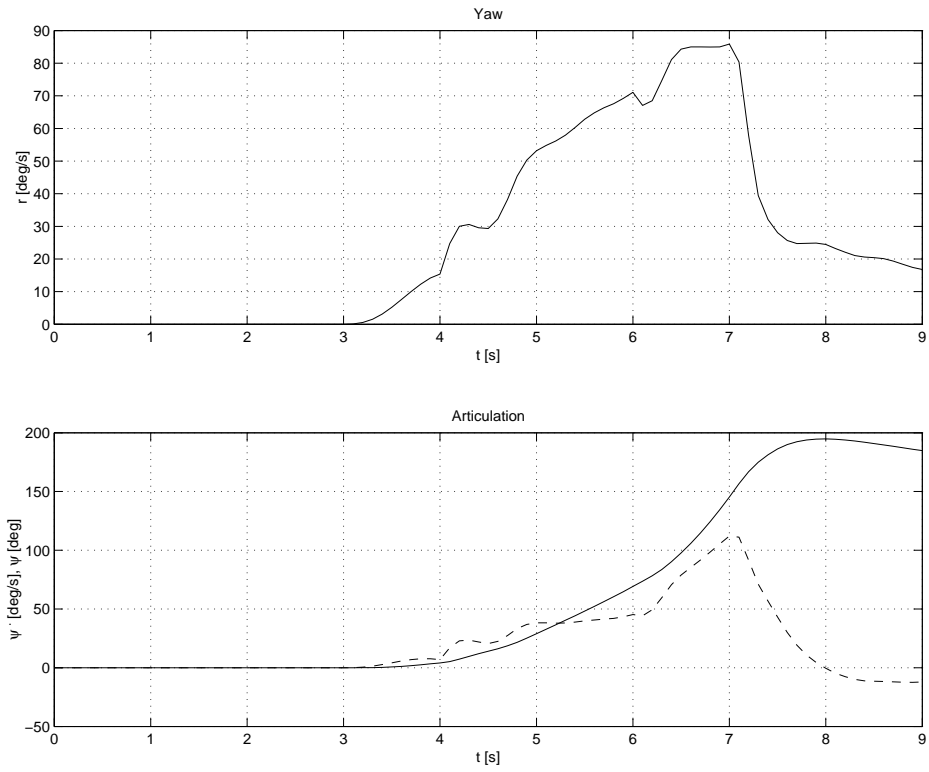
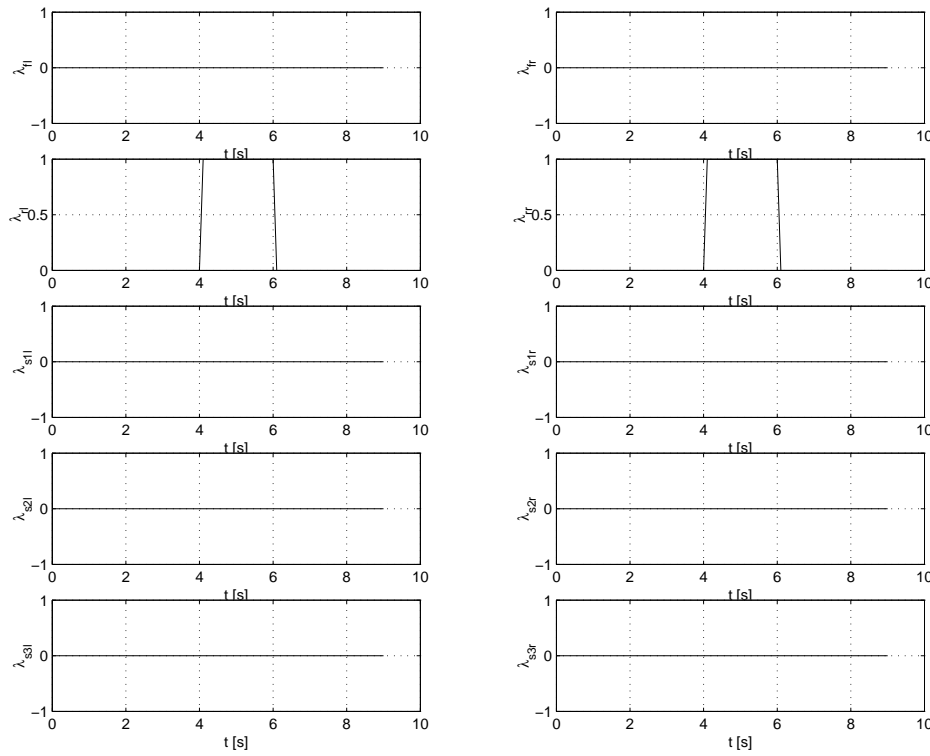**Figure 27** Yaw motion. (Solid: position; Dashed: velocity)
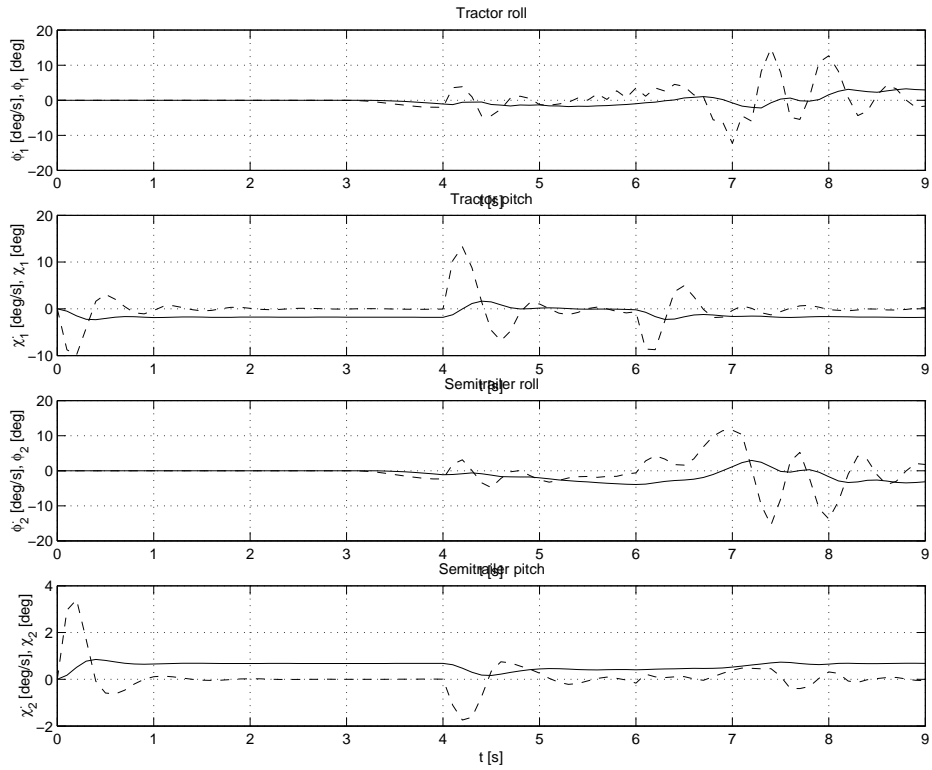
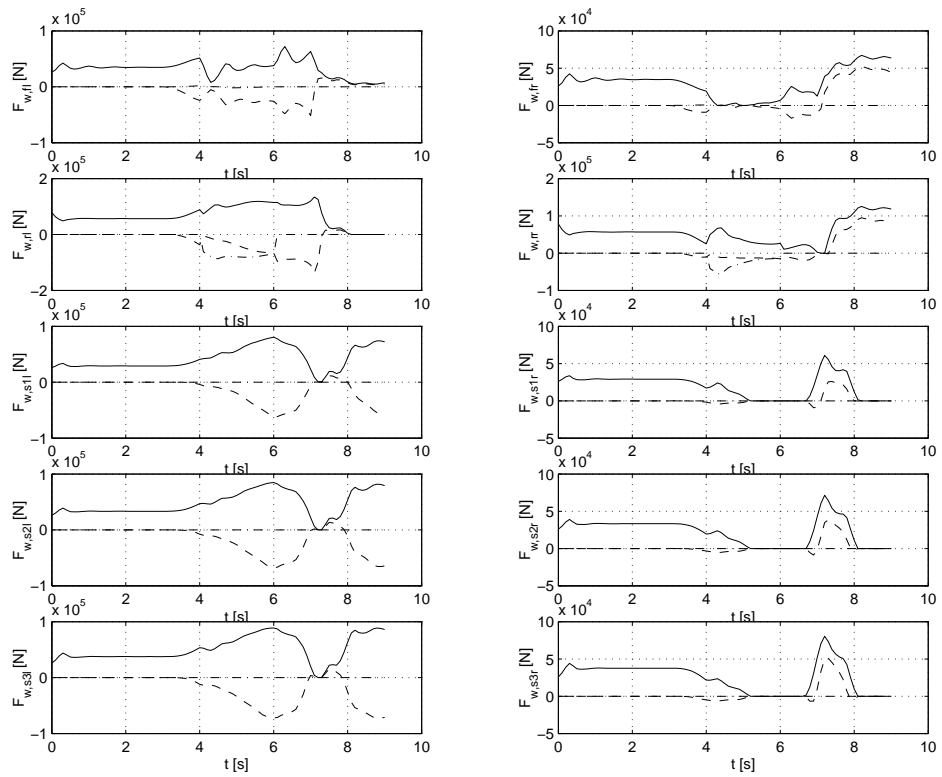**Figure 28** Roll and pitch motion. (Solid: position; Dashed: velocity)
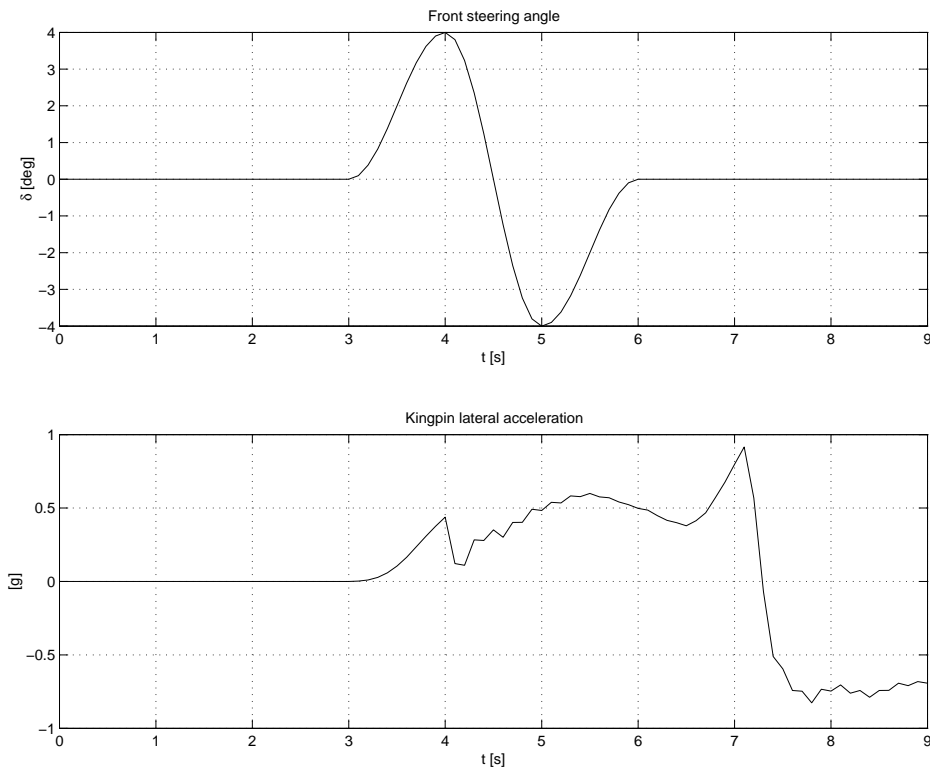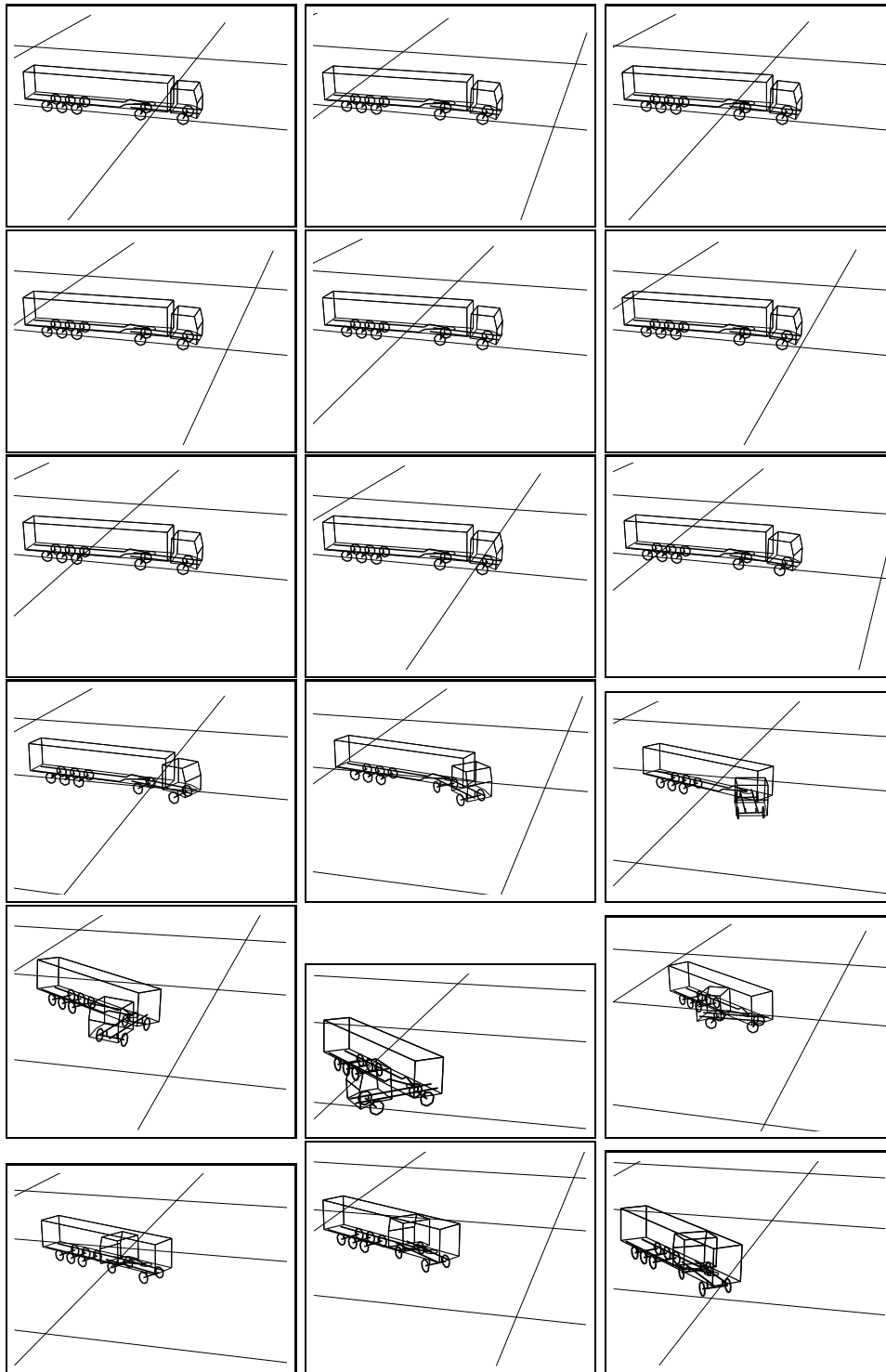
Figure 29 Steering input and lateral acceleration at kingpin.

Figure 30 Longitudinal slip inputs.

48

Figure 31 Tire forces in tractor and semitrailer unsprung reference systems respectively. (Dash-dotted: longitudinal; Dashed: lateral; Solid: vertical)

Figure 32 Matlab 3D-animation of the vehicle.